BUILDING BLOCKS FOR MULTI-HOP AND MOBILE AD HOC NETWORKS WITH FREE SPACE OPTICS

By

Jayasri Akella

A Thesis Submitted to the Graduate

Faculty of Rensselaer Polytechnic Institute

in Partial Fulfillment of the

Requirements for the Degree of

DOCTOR OF PHILOSOPHY
(CANDIDACY DRAFT)

Major Subject: Electrical, Computer and Systems Engineering

Approved by the
Examining Committee:

____
Shivkumar Kalyanaraman, Thesis Adviser

____
Partha Dutta, Member

____
Costas Busch, Member

____
Biplab Sikdar, Member

____
Murat Yuksel, Member

Rensselaer Polytechnic Institute
Troy, New York

December 2005
(For Graduation August 2006)

BUILDING BLOCKS FOR MULTI-HOP AND MOBILE AD HOC NETWORKS WITH FREE SPACE OPTICS

By

Jayasri Akella

An Abstract of a Thesis Submitted to the Graduate

Faculty of Rensselaer Polytechnic Institute

in Partial Fulfillment of the

Requirements for the Degree of

DOCTOR OF PHILOSOPHY
(CANDIDACY DRAFT)

Major Subject: Electrical, Computer and Systems Engineering

The original of the complete thesis is on file
in the Rensselaer Polytechnic Institute Library

Examining Committee:

Shivkumar Kalyanaraman, Thesis Adviser
Partha Dutta, Member
Costas Busch, Member
Biplab Sikdar, Member
Murat Yuksel, Member

Rensselaer Polytechnic Institute
Troy, New York

December 2005
(For Graduation August 2006)

CONTENTS

LIST OF TABLES

LIST OF FIGURES

ABSTRACT

Optical wireless, also known as free space optics (FSO) is a high bandwidth communication technology that enables information transmission through atmosphere using modulated light beams. FSO communication technology has attractive characteristics like dense spatial reuse due to light beam directionality, low power usage per bit, and license-free band of operation. FSO networks face two major challenges for deployment as general purpose metropolitan area networking or multi-hop ad hoc networks. They are: a need for the existence of line-of-sight between the communicating nodes and reduced transmission quality for adverse weather conditions. This thesis proposes new approaches in the physical and datalink layers to address above challenges and improve the link reliability. Further, motivated by higher layer issues like routing, we propose new methods of node localization and mobile tracking using FSO. These contributions are described below.

Spherically shaped omnidirectional optical nodes and auto-aligning electronic circuitry is proposed and implemented as a new solution approach to address the **line-of-sight alignment** problem. With this, not only the auto-alignment problem is addressed, but for the first time, we demonstrated high bandwidth **mobile FSO** communication. This opens up the possibility of a whole new application regime for FSO technology, auto-configurable mobile ad hoc networks.

Next, to address the reduced transmission quality due to adverse weather conditions, we propose to use short **multiple hops** of the FSO link. We analyzed the error behavior of multi-hop FSO link and showed that the error performance is better compared to a single hop link for the same end-to-end range. We also demonstrated that planar array antennas achieve high spatial redundancy/re-use provide very high aggregate bandwidth in short range FSO communication. In the data-link layer, we plan to implement suitable Forward Error Correction (FEC) codes to further increase the reliability of the FSO link.

We exploit the directionality of the FSO link, and propose a new method to achieve **distributed node localization** in an ad hoc network. With the proposed

method, we can achieve a relative coordinate system for the FSO network in a distributed manner. With our method, when the nodes move, they can self-compute the new coordinates by collaboration with the neighboring nodes enabling **mobile tracking**. In the datalink layer, we plan to implement a name-to-address mapping on the top of our localization scheme to enable stateless geographic routing on FSO nodes.

CHAPTER 1
Introduction

1.1 Motivation

Free space optics is a communication technology that enables information transfer through atmosphere using modulated light beams. Since the signal is transmitted without a wire, free space optics, FSO, is often referred to as "fiberless optics" or "optical wireless" transmission. FSO can provide full-duplex gigabit throughput for voice, video, and data information. FSO and fiber-optic transmission systems use similar infrared (IR) wavelengths of light and have similar transmission bandwidth capabilities. Furthermore, given the fact that the optical spectrum is unlicensed with frequencies of the order of hundreds of terahertz, FSO can be installed license-free world wide. Most FSO systems use simple ON-OFF keying as a modulation format, the same standard modulation technique that is used in digital fiber optics systems [6]. This simple modulation scheme enables FSO systems to provide bandwidth-transparent and protocol-transparent physical layer connections.

The directionality of light makes FSO a line-of-sight communication technology. Current FSO communication equipment is mainly targeted to provide communication between two points separated by a line-of-sight. For example, FSO is deployed between various buildings in a metro area, for intra-campus communication, media coverage, disaster recovery, and defense-sensitive communication providing bandwidths close to 100 Mbps per link. Commercial systems that cater FSO services (eg. Terabeam, Optical Access, Light Pointe) typically form a single primary beam and a few backup beams to operate in normal weather conditions. During adverse weather conditions, the link quality is restored with a lower bandwidth RF back up.

RF/microwave wireless, in comparison, can operate without a line-of-sight between the communicating nodes. Microwave communication systems operate at frequencies that are orders of magnitude lower than infrared communication systems. In general, frequencies above 1 GHz are considered to be part of the mi-

Communication technology	Free space optics	Millimeter-RF wireless	Optical fiber
Bandwidth	OC192 (9.6 Gbps)	OC12 (622 Mbps)	OC768 (40 Gbps)
Cost of Deployment	5-50K	5-50K	Very High
Concerns	Fog Absorption	Rain and Fading	Very Reliable
Distance	1.24 miles	3-12.42 miles	7-12.42 miles

Table 1.1: Comparison between various broadband technologies

crowave spectrum. Infrared laser communication systems operate in a frequency range around 200 THz, and hence can provide much higher bandwidth. On the other hand, RF/microwave can provide a more robust wireless communication links in adverse atmospheric conditions. It is fair to say that these two wireless technologies compliment well with each other that hybrid RF/FSO technology can provide a realistic solution for broadband access problem. A comparison of the characteristics of these two technologies is given in Tabel 1.1.

The objective of this thesis is to understand the merits and limitations of FSO technology for use in general purpose local and metropolitan area networks. We believe that FSO has several attractive characteristics that make it suitable not only for last mile access networks, but also for mobile ad hoc and large range multi-hop networks. They are:

- **Directionality of the light beam.**

  The light beams used for FSO communication are much narrower and typically have an angular width of 1 milli radian, as opposed to omnidirectional RF, which occupies 360^0 in a plane. Because of this there are generally no interference issues in FSO communication and there are no or very little medium access issues.

  Directionality also helps in localization, because it is very easy to get orientation information of the neighbor, unlike RF, where phased array antennas are needed to have such capability. Coupled with range information, FSO technology can be effectively used to simplify the process of node localization in an ad hoc network.

- **Form Factors, i.e., Size and Power per bit.**

The size of the equipment used for short range (up to 500 meters) FSO communications can be as small as a laser pointer (i.e., a few centimeters). This makes dense integration of multiple FSO transceivers on to a single physical structure, for example a 1×1 sq.ft. array or a 1 cu.ft. sphere. In this thesis we propose the design of such structures to achieve angular diversity for alignment, mobility, and ultra-high bandwidths. Semiconductor lasers and LEDs used for FSO communications use very little power (a few milli-watts) making it suitable for power limited ad-hoc and sensor network scenarios. This also makes it practical to realize multi-hop networks to improve the link quality and further reduce the power needed, because the cost of deployment of relaying hops is small.

- **Ability to be operated license-free worldwide and quick installation.**

  Optical wavelengths are license free, so FSO deployment does not require any permissions as long as they are eye safe. The FSO systems can be deployed in an ad hoc manner, typically can be installed in a single day. Also,the system can be made to operate behind transparent windows, avoiding expensive roof top rights.

1.1.1 Challenges

Originally developed by the military and NASA, FSO has been used for more than three decades in various forms to provide fast communication links in remote locations. For general purpose applications, FSO is still a niche technology serving commercial point-to-point links in terrestrial last mile applications [31], [1], [24] and in infrared indoor LANs. FSO faces two major challenges for deployment as a general purpose metropolitan area networking or multi-hop ad hoc networks. They are: a need for the existence of line-of-sight between the communicating nodes and reduced transmission quality for adverse weather conditions. In this thesis we address the above two challenges with a single objective, improving the link reliability. These challenges are described in detail below:

1.1.1.1 Need for Clear Line-of-Sight and Alignment

Since FSO is a line-of-sight (LOS) technology, nodes communicating with each other must be free from physical obstruction and able to always "see" each other for communication to proceed. Flying birds and construction cranes can temporarily block a single-beam FSO system. Link reliability can be increased using multi-beam systems (spatial redundancy/re-use) combined with spatial coding techniques to overcome temporary obstructions, as well as other atmospheric conditions.

Apart from having a clear line of sight, constant *alignment* is called for for maintaining smooth operation of FSO systems. Building sways and seismic activities constantly mis-align the sender and the receiver. LOS scanning, tracking, and alignment have been studied for years in satellite FSO communications [20], [37], [10]. These works considered long-range links, which utilize very narrow beamwidths (typically in the microradian range), and typically use slow, bulky beam-scanning devices, such as gimballed telescopes driven by servo motors.

In this thesis we address the LOS alignment through interesting spatial structures that are amenable to auto-tracking and auto-configuration using intelligent electronics.

1.1.1.2 Atmospheric Effects

In FSO the medium is free space and so optical wireless networks based on FSO technology must be designed to overcome changes in the atmosphere. The transmission quality reduces in adverse weather conditions, and during foggy conditions, the signal attenuations as high as 300db/Km, make the link totally unavailable. Current terrestrial FSO links using lasers are limited to a range of a few kilometers [65], though satellite communication has routinely used FSO links ranging several thousands of kilometers. The terrestrial limitations occur primarily due to atmospheric attenuation (fog, rain, snow, etc) and geometric attenuation (due to beam divergence). Considerable FSO work especially in industry has been on characterizing link availability under various atmospheric conditions [35], [34], [60], [41], [19] with higher availability in clear-conditions towns like Las Vegas and poor availability in towns with dense fog conditions like St. Johns.

The primary challenge for FSO-based communications is dense fog, as the size of particles in fog is comparable to the wavelength of the light used to transmit the signal. Rain and snow have little effect on FSO technology. The primary solution to counter fog when deploying FSO-based optical wireless products is through a network design that shortens FSO link distances and adds network redundancies. FSO installations in extremely foggy cities such as San Francisco have successfully achieved carrier-class reliability.

In comparison, microwave transmission is more affected by rain compared to fog because its wavelength is close to size of raindrops. Lower frequency RF transmission (e.g.: 802.11x, 802.16) is relatively unaffected by such atmospheric effects, and does not require LOS for link availability. But it has significant attenuation due to vegetation, concrete walls, etc. Multi-path fading and interference combined with limited frequency spectrum pose signal processing challenges at such lower frequency RF ranges. Note that interference is not a significant problem in FSO transmission.

1.1.2 Potential Possibilities

The solutions we propose in the physical and datalink layers are motivated by the higher layer issues like auto-configuration and routing. For example, we exploit the directionality of the FSO technology to come up with a new localization and mobile tracking schemes, which will enable stateless geographic routing. Those new applications of FSO technology are described below:

1.1.2.1 Ad Hoc Network Localization

The directionality of FSO can be usefully exploited to simplify ad hoc network localization and mobile tracking. Current localization techniques use triangulation, either using GPS or GPS-free techniques, to obtain node positions in an ad hoc network. Triangulation calls for a very high node density to achieve good coverage of localization, which cannot always be guaranteed in an ad hoc setting. On the other hand, using FSO technology, nodes can find relative orientations and ranges from each other, and compute the positions as a simple vector addition in a distributed

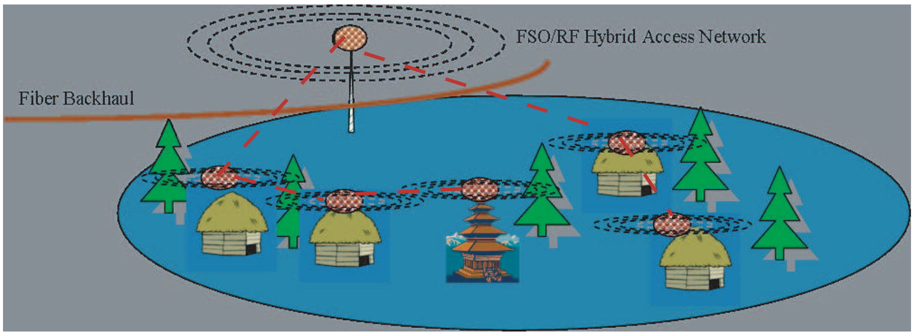

Figure 1.1: FSO/RF Hybrid Last Mile access.

manner. This method guarantees 100% node localization when the underlying graph is connected.

1.1.2.2 Mobile Tracking

The node localization mentioned in the previous subsection can be easily extended to track mobile nodes. We propose a technique in where nodes can compute the new coordinates after movement by collaborating with neighboring nodes in the new location. With this method, we can implement a distributed mobile tracking, without depending on any central infrastructure.

1.2 Contributions of the thesis

1.2.1 Angular diversity for Line-of-sight Auto-alignment and Mobile FSO

We proposed, designed, simulated, and prototyped 3-dimensional omnidirectional spherical antennas to address the line-of-sight alignment problem in FSO communication using angular diversity of such structures. Spheres of appropriate size tessellated with multiple optical transceivers coupled with smart electronics can auto track line-of-sight between moving FSO nodes. We describe the details of this approach in the Chapter 3. We also demonstrated that 3-D spherical antennas are the enabling technology to realize mobile FSO nodes and achieve reasonably reliable communication between them.

1.2.2 Spatial Re-use for high bandwidth and link reliability

We demonstrated that 2-dimensional arrays of FSO transceivers give excellent bandwidth performance over short range free-space optical (FSO) communications. Multiple hops of short-range FSO channels can be easily implemented in a LAN environment. For example, in an indoor access network or a campus-wide LAN scenario, we can tremendously increase the bandwidth by using 2-dimensional arrays. By choosing the appropriate design parameters, the inter-channel interference in these 2-D systems can be reduced. The details of this work are described in Chapter 4. Further, we plan to use the spatial redundancy/re-use offered by such arrays to improve the reliability of the FSO link using suitable forward error codes.

1.2.3 Error Analysis on Multi-hop FSO links to improve link reliability

We demonstrated that error performance of the multi-hop free space optical communication is better than single hop communication for the same end-to-end link range and the same end-to-end power. We showed that the mean error rate in the case of multi-hop communication is smaller than that of the single hop equivalent, for both clear weather and adverse weather conditions.

More importantly, the variance of the error rate is significantly smaller for multi-hop operation. This narrow variance of the error helps to design effective FEC codes for the multi-hop network, which we plan to implement in the future. This approach is more energy efficient since fewer bits need to be transmitted and the range of the target error rates is smaller as compared to single hop operation. The decrease in the mean error and variance with the number of hops is presented more in detail in Chapter 5.

1.2.4 Node Localization

We demonstrated a localization scheme that achieves a relative coordinate system for an ad-hoc network in a distributed manner. The scheme achieves 100% node localization when the underlying graph is connected, irrespective of the average node degree or node density. We evaluated the performance of the algorithm in terms of the coverage (extent of localization), number of iterations, and control messages needed to achieve the relative coordinate system. We also compared these metrics for a scheme that uses triangulation for localization and showed that our scheme performs better. We simulated the error in localization due to measurement errors in range and orientation and its propagation with the number of hops from the origin.

Our localization method can be easily extended for mobile tracking. Nodes, after they move, collaborate with their new neighbors and jointly come up with their new coordinates. We plan to implement a name-to-address mapping for this localization so as to do geographic routing. The node localization method and mobile tracking approach are presented in Chapter 5.

1.3 Organization of the Thesis

In Chapter 3 we describe a novel antenna design for FSO nodes that addresses the line-of-sight alignment problem. In Chapter 4, we describe how multi-element array antenna can achieve higher aggregate bandwidth even after the presence of inter-channel interference. The chapter also discusses the design guidelines for such array antennas. In Chapter 5, we present the benefits of having a multi-hop FSO link over single hop FSO link in terms of the transmission errors and energy gain. In Chapter 6, a new localization scheme based on FSO technology is presented. The chapter also discusses how mobile tracking is achieved without any central infrastructure. Finally in Chapter 7, the future directions are presented.

CHAPTER 2
Literature Survey

Prior research on FSO focussed on auto-tracking of the line-of-sight for single transmitter and single receivers (though there are some commercial systems available with multi-transmitters [41]), channel error characterization in turbulent atmospheric conditions [31], device characterization for the light sources and receivers, signal processing to overcome atmospheric effects, and indoor diffuse optical systems. Auto-alignment combining angular diversity and electronics, increased bandwidth and reliability due to spatial redundancy/re-use, multi-hop error analysis, and ability of FSO in node localization were never addressed before. This thesis considers those issues.

There are applications of FSO in intra-chip communication targeted to increase the speed of operation, but that discussion is not within the scope of this thesis. Current FSO communication equipment is targeted at point-to-point links (though some preliminary multi-hop proposals exist [1], [67] using high-powered lasers and relatively expensive components used in fiber-optical transmission. The focus of these commercial systems (eg. Terabeam, Optical Access, Light Pointe) is to form a single primary beam (and some backup beams) with limited spatial re-use/redundancy and to push the limits of operating range, and to improve link availability during poor conditions.

2.1 Line-of-sight auto tracking

LOS scanning, tracking and alignment have been studied for years in satellite FSO communications [20], [37], [10]. These works considered long-range links, which utilize very narrow beamwidths (typically in the microradian range), and which typically use slow, bulky beam-scanning devices, such as gimballed telescopes driven by servo motors.

Alignment of LOS is a critical issue in FSO communications. In currently installed commercial FSO systems, alignment is usually done manually [65], [44] using aids like telescopes and mechanical auto-tracking techniques. These techniques have low alignment tolerances and, most often a rigid mounting is expected. Feedback-based auto-alignment that uses a mixture of electronic and mechanical techniques is usually available at higher cost. But, a simpler solution used is to make the conical optical beam wider at transmission: even with sway, the receiver would remain in the sender's beam [41]. This solution requires higher transmission power. With 1micron divergence, at a distance of one kilometer from the laser, due to geometric dispersion, the diameter of the beam is about one meter on a self-aligning system and can be three to six meters on a non-self aligning system. Dependency on the line of sight between the sender and the receiver imposes a lot of restriction on the mobility of both. There are several solutions proposed in literature based on spatial redundancy and diffuse light sources and tracking etc. [37]. The tolerances given by the spatial redundancy methods are usually very small and they hardly can provide any practical mobility. The diffuse system ranges are very limited; usually they are used within a single room [24].

It is interesting to note that non-LOS optical operation is possible under certain conditions (eg: indoor infrared). For example, though Infrared Data Association (IrDA) standards [31], [26] are primarily for short-range, half-duplex LOS (a.k.a Point-and-Shoot) links, they allow non-line-of-sight (non-LOS) operation, but only within a single room (very short distance of 1-10m, within a half-power angle of at least 30^o), expecting the availability of multiple reflected LOS paths. This operation is called diffuse link operation. Our research is different from short range diffuse systems. We focus on directed, long range multi-hop FSO systems.

IrDA's Advanced Infrared (AIr) is a physical layer that supports robust links within a 120^o horizontal half-power angle at data rates between 250 kb/s and 4 Mb/s. Indoor infrared also requires stringent eye-safety requirements: IEC Class 1 allowable exposure limit (AEL) [29].

Though IrDA standards have been incorporated into hundreds of devices, unlicensed RF-based wireless networking is attracting explosive interest today for non-LOS wireless data communication. IEEE 802.11b and 802.11a WLAN standards have been out since 1997 and 1999 respectively [21], [27]. Very low cost WLAN technology components that operate at rates of up to 11 Mbps (802.11b) and 54-108 Mbps (802.11a) are widely available in the market place. Though 802.11b was intended for WLAN (short range) purposes, community network initiatives based upon 802.11b are growing rapidly [18]. The IEEE has also recently ratified 802.16a and 802.16 standards (see for the frequencies 2-11 Ghz and 11-66 Ghz respectively, primarily intended as wireless metropolitan area network (WMAN) standards. However, low-cost products in this space for various unlicensed spectra (eg: 57-64 GHz) have yet to appear on the marketplace. We strongly believe that the deployment of cheap, open-standards based unlicensed spectrum products using meshed multi-hop architectures and IP-based routing will finally break the last-mile bottleneck [57]. The success of RF-alternatives (802.11b in particular) has kept most of the research community focus on RF-based open standards technologies. Our multi-hop FSO scheme aims to extend the success of unlicensed RF standards, by focusing on cheap, ultra-high-speed (100Mbps-10 Gbps+) capabilities in the last-mile.

2.2 Spatial Re-use/Redundancy

Multi-channel operation in FSO interconnects, which communicate over very short distance (e.g. cms), has been well studied [50], [58], [62], [61], [7], [33]. However, consideration of multi-element FSO communication over longer distances has not been investigated. In the last decade there has been tremendous amount of research in mobile ad hoc networking issues, especially routing, and antenna design to improve the capacity [28], [23], [39], [22]. Technologies like 802.11G provide a max of 20-50 Mbps depending upon implementation serving the ad hoc networks and the last mile wireless networks. An open problem is to scale this capacity by several orders of magnitude while retaining the ad hoc aspects so as to serve emerging high bandwidth military and civilian applications. It's been shown that multi-element antennas improve capacity as many times as the number of elements on the antenna [12].

A key benefit of FSO is that interference issues in optical wireless can be largely addressed by manipulating system parameters like operational range, divergence, and by simple engineering designs like parabolic mirrors etc. This stands in stark contrast to RF that is prone to interference and needs additional computational complexity (signal processing) to combat it. With RF-technologies, a well-known fundamental limit on the capacity of ad-hoc networks has been enunciated by [23], and subsequent work by [30] have shown that real ad-hoc networks using 802.11 fall well below the theoretical limit (though [22] have shown capacity improvement with mobility). It can be noted that, in FSO, by improving each of the factors comprising the BV product, we can improve the speed. For example, high-speed LED/PD pairs can increase the bandwidth offered by each channel, range of operation can be increased using longer wavelengths like 10 Micron. And by reducing the divergence, the density of the spatial integration of the optical transceivers can be increased, increasing the overall system capacity.

In commercial FSO systems, lasers in the 850nm and 1550nm band are preferred due to superior propagation characteristics in this band and higher power budget due to low geometric dispersion [65], [35]. Such equipment would be very costly and demands high-power [4] in the context of multi-element scenario. Moreover, such laser-based equipment would not have the form factor, weight and power characteristics to be mounted on ad-hoc infrastructures. We instead used LEDs in our design as they are more amenable to dense spatial integration, have longer life than lasers, and fewer eye-safety regulations [66]. High-brightness LED technology is being rapidly developed in the context of solid-state lighting (see [55], [63], [2]. LEDs can be internally modulated at rates up to 2Gbps [4], and spatial integration of hundreds of such LEDs can increase the aggregate capacity to multiple Tbps. The divergence can be managed to some extent with parabolic micro-mirrors or micro-lens packaging. But the spatial integration gains achievable using LEDs are huge. Recently, wireless communications using high speed LEDs have been reported [45] and several optimizations to their setup is possible for higher bandwidth operation.

2.3 Angular Diversity

Leveraging of spatial and angular diversity techniques for FSO communication had been reported earlier to address small mis-alignments and low SNR etc [59]. Indoor diffuse systems have angular diversity built into the system, making

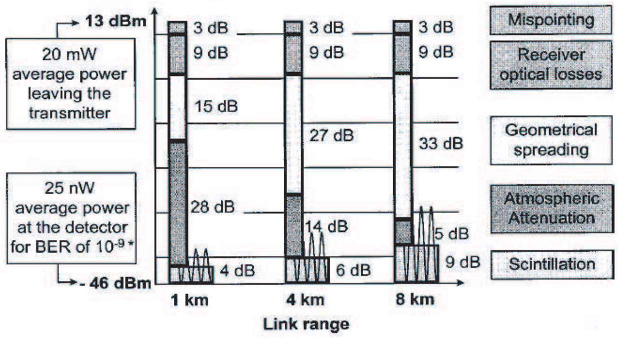

Figure 2.1: FSO link budget from [34]

alignment simple. But those systems have very limited range, usually within a room [24]. Research has been done to use angular diversity of a specially designed receiver structure, hemi-spherical, to combat for mis-alignments. But other than small motions and displacements, angular diversity is not applied to achieve *mobility* in FSO.

2.4 Atmospheric Effects on the Link

Current FSO links using lasers are limited to a few kilometers [65], though satellite communications has routinely used FSO links ranging several thousands of kilometers. The terrestrial limitations occur primarily due to atmospheric attenuation (fog, rain, snow etc) and geometric attenuation (due to beam divergence). Considerable FSO work especially in industry has been on characterizing link availability under various conditions [35], [34], [60], [41], [19] with higher availability in clear-conditions towns like Las Vegas and poor availability in towns with dense fog conditions like St. Johns. A sample link budget used in laser-based systems is shown in Figure 2.1 and Figure 2.2 [34]. Dense fog affects optical transmission far more than other conditions. An average of 99.98availability for FSO, and microwave RF backup can provide even higher (carrier-class) availability percentages (eg: 99.999%).

The atmospheric effects on the FSO link can be classified as below:

- **Fog:** Fog is vapor composed of water droplets, which are only a few hundred microns in diameter but can modify light characteristics or completely hinder the passage of light through a combination of absorption, scattering, and

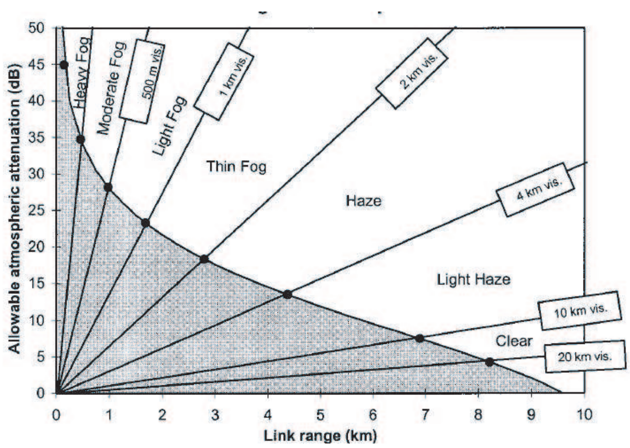

Figure 2.2: Effect of Atmospheric conditions from [34]

reflection. Fog causes worst signal loss in FSO systems. From moderate fog onwards, FSO link is totally lost, and call for a RF back-up.

- **Absorption:** Absorption occurs when suspended water molecules in the terrestrial atmosphere extinguish photons. This causes a decrease in the power density (attenuation) of the FSO beam and directly affects the availability of a system. Absorption occurs more readily at some wavelengths than others. However, the use of appropriate power, based on atmospheric conditions, and use of spatial diversity (multiple beams within an FSO-based unit) helps maintain the required level of network availability.

- **Scattering:** Scattering is caused when the wavelength collides with the scatterer. The physical size of the scatterer determines the type of scattering. When the scatterer is smaller than the wavelength, this is known as Rayleigh scattering. When the scatterer is of comparable size to the wavelength, this is known as Mie scattering. When the scatterer is much larger than the wavelength, this is known as non-selective scattering. In scattering unlike absorption there is no loss of energy, only a directional redistribution of energy that may have significant reduction in beam intensity for longer distances.

- **Scintillation:** Heated air rising from the earth or man-made devices such as heating ducts create temperature variations among different air pockets. This can cause fluctuations in signal amplitude which leads to "image dancing" at the FSO-based receiver end.

2.4.1 Multi-Hops on FSO

To combat the attenuation effects of geometric spreading and atmospheric losses, and increase the reliability of an FSO link, two important methods have been proposed in the literature [1], [17]. In [17], performance increase by providing hybrid link protection using an RF backup is proposed. In [1], by scaling the hop length down between the transmitter and receiver and by using multi-hop routing, higher link availability is achieved.

2.5 Localization

Applications of FSO other than single hop communication and intra-chip communications are not explored in prior work. We propose a new application for FSO, node localization in an ad hoc network. We describe the existing localization techniques that typically use RF and a combination of RF and ultrasound.

The problems in distributed localization can be broadly categorized into three layers. The lowest being the localization scheme to obtain the coordinates of the nodes, the second layer to map the node "identification" to it's physical location (eg. Geometric Hash tables) and the third layer to implement geographic routing. In this section we will discuss the previous work done in the first layer, i.e., distributed localization schemes.

Depending on the application and the context for which location information is used, there are several types of location systems that exist. For example in sensor network applications, real location of the sensor is needed to meaningfully interpret the data. On the other hand, for peer-to-peer applications on the wired network, location information in terms of the "connectivity" is enough, which is given by the virtual coordinates in the network graph. A third method based on robotic methods uses vision /sensor data where the algorithm has a prior training to construct a location map. [25] reviews a host of location systems, that work with centralized infrastructure or in a distributed manner. In this paper we do not discuss robotics based methods, as they need extensive computation and signal processing to obtain

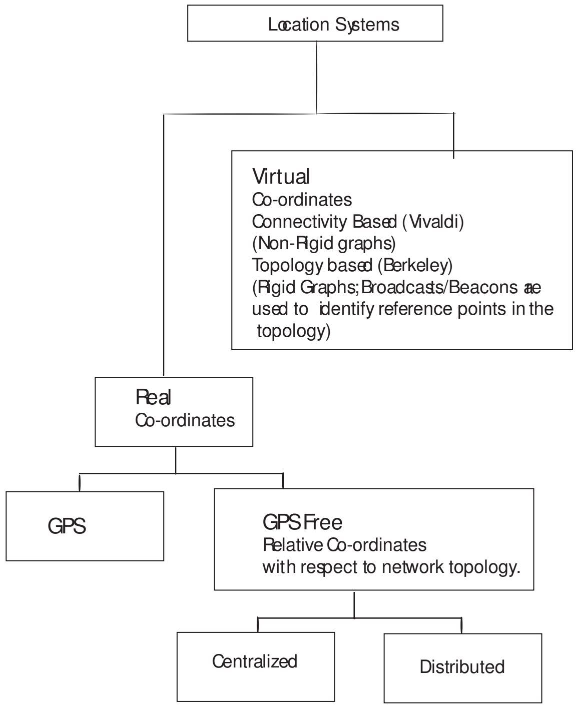

Figure 2.3: Taxonomy of various location systems

location data which is not suitable for ad hoc and sensor network scenarios.

The most popular method of obtaining location information is using GPS (Global Positioning System). GPS is an *absolute physical* positioning technology, providing absolute global position of the objects. GPS provides lateration framework with coverage using worldwide satellite constellation. GPS receivers use universal transverse mercator coordinates to compute and report their location with in 1-5 meters using the Wide Area Augmentation system of GPS. The computation of GPS is *localized*, protecting the privacy of the receivers/mobile devices with increased computational burden on these devices. Because of the high cost and need for infrastructure, GPS is not entirely suitable for positioning in ad hoc/sensor network environments. In [36] a system that achieves indoor localization using only RF signal strength as measured by an IEEE 802.11b wireless ethernet card communicating with standard base stations.

In the following we broadly categorized and briefly reviewed previous work on location systems as shown in Figure 2.3.

Typically in a geographic localization scheme an estimate of “distance” is obtained either by the number of *hops* or an RTT, or an explicit *range* or *orientation* to compute the virtual or physical (absolute or relative) coordinates respectively. In literature, three kinds of node coordinates are proposed and are discussed below.

The first one, as described in [16] "virtual coordinates" for the nodes are obtained based on the underlying connectivity of the network but not true geographic distances. The primary objective of these coordinates are to find servers which are located closer to the client, for example, in a peer to peer application. The method piggybacks on the existing traffic to get RTT data to another node which is used to compute the coordinates. The authors proposed a "height vector" which represents the access delays experienced by the nodes so as the coordinates accurately represent the total RTT between two nodes. The goal is to accurately predict RTT under changes in the network and use that information for server selection, rather than "geographic routing". How mobility is implemented for such systems is not specified. [48] proposes another virtual coordinate localization scheme used for geographic routing. This method identifies perimeter nodes using beacons placed in the middle of the ad hoc network. The beacons and the identified perimeter nodes perform broadcast operations so triangulation for the number of hops can happen at regular nodes and within the perimeter nodes. The power of such systems is that geographic routing is achievable without the "actual" location information. The authors addressed mobility of the nodes and showed that the system does not perform as well as for non-mobile case.

The second type of coordinates are "global geographic" coordinates consistent with GPS when only a small subset of the nodes in the network has GPS information. These systems rely on range or orientation estimate with the one hop neighbors and hence are completely distributed. In [43] a distance-vector based technique that uses "orientation forwarding" to obtain localization is proposed to use with mapping and Geodesic routing. This technique uses angle of arrival to triangulate. With this method, even when only a fraction of nodes have global positioning information, location information is propagated hop-by-hop and network localization is achieved. This system can handle mobility with the mobile node communicating with it's one hop neighbors to triangulate and compute it's new position. This is possible because of the presence of a few GPS aware nodes in the network. Another similar technique is proposed by [52] by cooperative ranging between nodes used with TERRAIN (Triangulation via Extended Range and Redundant Association of intermediate Nodes) approach to localize and reduce localization errors due to range measurement errors.

The third type "relative geographic" coordinates in GPS-free networks for location aided routing or Geodesic forwarding. These techniques typically result in a coordinate systems with respect to the network topology, and hence are relative. For example [9] provides a relative coordinate system by each node from the knowledge of the distance from their one hop neighbors. Each node builds its local coordinate system with itself as the origin and the first hop neighbors. And in the second stage each node broadcasts to build a network coordinate system by aligning the axes of all the nodes. The range or orientation estimates are obtained by several techniques, to name a few, time of arrival $\underline{T}OA$ where prior synchronization is made and based on the timestamp of the arrived signal, range estimate is obtained. Time difference of arrival, which exploits the speed difference between acoustic and RF signals. Both are sent at the same time from the transmitter and the receiver measures the time difference of arrival and computes the distance/range, angle of arrival, and signal strength. To handle node mobility, a high density region in the network is made the reference group with respect to which all the node coordinates are computed in the event of a motion.

Typically in all these techniques, a range or orientation estimate is used and triangulation is performed by each node, so these techniques assume a node density that can support it. Typically, this node density is much higher than needed for simple connectivity of the network. [11] showed that these single parameter r-only localization and optimizations schemes require 3- connectedness, which occurs only at high densities. They propose to make use of both the range and the bearing ability to nodes to improve on both the density and placement of the anchor requirements of the localization schemes.

Our work is very closely related to [11]. We propose to use two parameters or localization, r and θ instead of a sector. Corroborating [11], we show that r-only or θ - only techniques are equivalent and both require very high node densities to achieve localization. We show that using FSO technology, we can implement the nodes with those capabilities. In addition, we show that these two parameter technique is robust to topological changes in the network as well as node mobility.

CHAPTER 3
Spherical Optical Antenna: Line-of-Sight Auto Alignment and Mobile FSO Communication

In this chapter, we focus on the problem of line-of-sight auto-alignment critical in the Free Space Optical networks. We leverage the angular diversity offered by the multi-element 3-dimensional designs to not only solve the auto-alignment problem, but also to achieve *mobility*. This leveraging of spatial and angular diversity techniques for FSO communication had been reported earlier to address small mis-alignments and low SNR etc [59]. Given the limitations of FSO communications for its need to depend upon clear line-of-sight between the communicating nodes, FSO was never before considered for mobile applications. With our solution approach to that problem, we report the possibility of mobile FSO communications for low-to moderate speeds for the first time [1].

In this chapter, we show through experimentation and simulations that dense spatial integration of very inexpensive optical components (eg. LEDs/VCSELS) onto novel spherical structures embedded with smart electronics can provide angular diversity necessary for reliable optical connectivity even when the nodes are mobile. When the spheres move relative to each other, the electronic design allows rapid handoff of FSO channels thereby facilitating high-bit-rate communications even in mobile conditions.

The chapter is organized as follows: In Section 3.1, we describe the basic Free Space Optics Communication System. In Section 3.2, we describe the novel design of spherical optical antenna and the coverage analysis in terms of its parameters. In Section 6.2.4, we present the details of the alignment circuit that is designed to work with the spherical optical antenna. In Section 3.4, we present the experiment we performed to illustrate the mobile FSO connectivity. In Section 3.5, we present the NS simulations we have performed to understand how well FSO mobile communication works with Mobile-IP for UDP traffic. Section5.6 concludes with future

[1]The results in this chapter are joint work with Murat Yuksel, David Partyka and Chang Liu

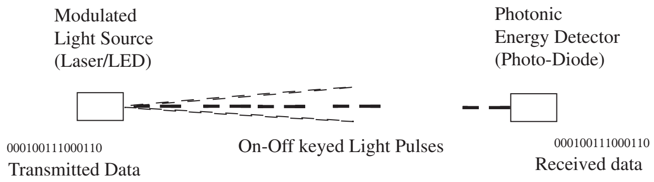

Figure 3.1: FSO communication system.

directions for this work.

3.1 Basic FSO System Description

The basic FSO communication system is shown in Figure 6.2. Typical systems have a single transmitter and a single receiver, in line-of-sight with each other are placed with in the operating range. The transmitter is a modulated light source, typically a low-powered laser operating in infrared band. The receiver is a photo-detector, and outputs a current proportional to the received light intensity.

FSO communication supports duplex connection, therefore both transmitter and receiver are present at both the ends. We call each end an "optical transceiver", which can both transmit and receive at the same time. An optical transceiver can be characterized by the transmitted light intensity I, an angle θ and receiving sensitivity η. The angle θ is the divergence angle of the laser beam. The intensity of the light varies across the cross section of the light beam [65] following the Gaussian beam profile. The intensity I_Y at a radial distance Y from the axis at a distance Z from the laser is given by:

$$I_Y = I_o e^{-\left(\frac{2Y}{W_z}\right)^2}$$

where I_o is the intensity at the center of the light beam and W_z is the diameter of the laser beam at distance Z. As seen in Figure 3.2, the intensity of the laser beam falls exponentially across the cross section.

The light beam from the transmitter is modulated to carry the signal digitally. Typical modulation scheme is On-Off Keying (OOK) digital modulation method, though there are proposals of using PP etc. In OOK, the carrier (light beam) is switched on to transmit a *ONE* and switched off to transmit a *ZERO*. At the receiver, the photo-detector operates in a threshold detector mode to receive the signal. If

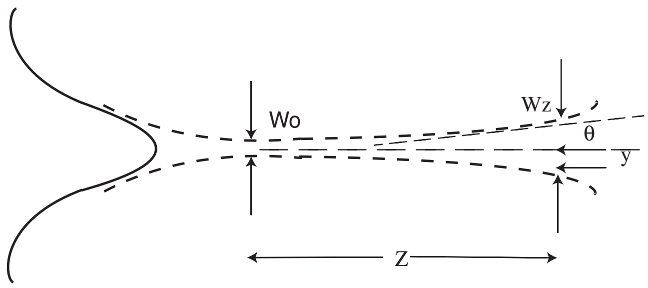

Figure 3.2: Laser Beam Profile.

the received light intensity is greater than a preset threshold I_T, then the detector outputs a *ONE* and if the received light intensity is smaller than I_T, the detector outputs a *ZERO*.

In a single channel, the output signal at the receiver can be written as $y = \eta I + \zeta$ where the intensity I is received from the transmitter, and η is the receiver sensitivity, and ζ is the Gaussian noise. When the received intensity $I \geq I_T$, $y = ONE$, otherwise it is a *ZERO*.

3.2 Concept of Tessellated Spherical Optical Antenna

The very geometrical shape of a sphere suggests spatial and angular diversity. We tessellated the surface of a sphere using optical transceivers each of which contains an LED (Light Emitting Diodes) as the transmitter and a photo detector (PD) as the receiver. Since LEDs have relatively high divergence angle and PDs have a comparable angular field of view, the LED-PD pair forms a transceiver cone. This cone covers a significant volume of 3-dimensional space. As shown in Figure 3.3, a sphere tessellated to an appropriate density can cover entire 360 steradian of the surrounding space. As seen from the figure, when the spheres move relative to each other, an existing LOS between them is lost and a new one is established.

In spherical FSO nodes tessellated with multiple optical transceivers, there are tradeoffs involving (i) interference (or crosstalk) between the neighboring transceivers, (ii) aggregate coverage area achieved by the FSO node, (iii) packaging density of the optical transceivers, and (iv) communication range. Therefore, higher packag-

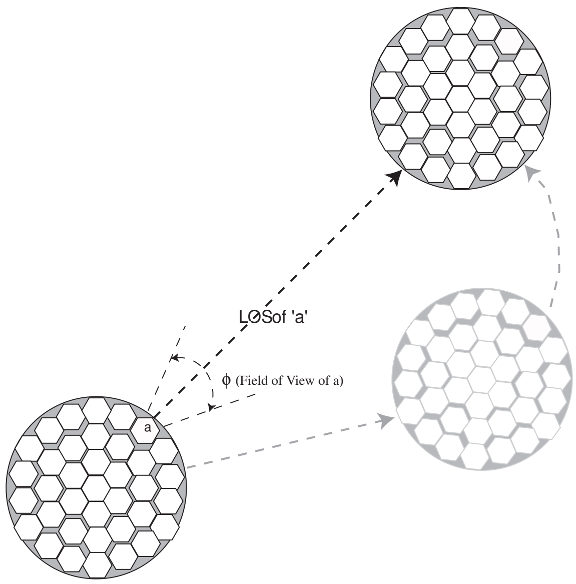

Figure 3.3: Two Spherical antennas tessellated with LED/Photo-Detector pairs in motion

ing density provides higher aggregate coverage but also increases the interference of the neighboring transceivers. An important design question is to ask how dense the packaging should be so that highest (or optimal) possible aggregate coverage is achieved without causing interference. In the next subsection, we present the analysis on the optical coverage that can be achieved using spherical optical antennas.

3.2.1 Spherical Antenna Coverage Analysis

In this section, we present our analysis of the scalability of the angular diversity and spatial reuse provided by a circular shaped FSO node. In particular, we answer the question of how much coverage can be achieved by a 2-d circular FSO node with the highest possible number of transceivers. The coverage area here refers to the area around the node, in which a communication link can be established with another node standing within the area of consideration. To find the optimal number of transceivers maximizing the total coverage of a 2-d circular FSO node, we first develop the model for total coverage area of such a node. Then, we devise an iterative algorithm to find the optimal number of transceivers that maximize the total coverage.

For a 2-d circular FSO node, the total coverage is dependent on the effective

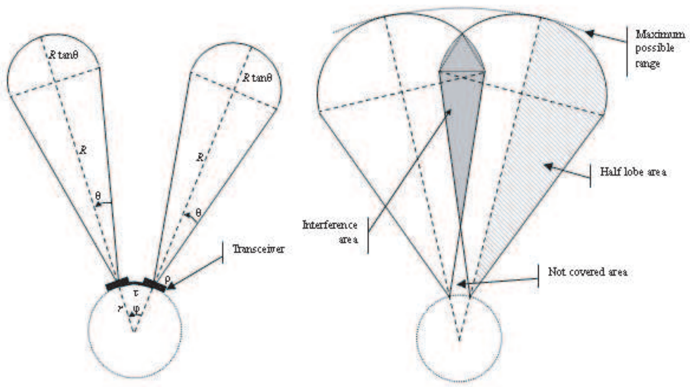

Figure 3.4: Coverage areas of the neighboring transceivers

coverage area achieved by a single transceiver C, and the total number of transceivers n. The effective coverage area of a single transceiver can be formulated based on two different possibilities of placing of the transceivers, as shown in Figure 3.4.

Let r be the radius of the circular 2-d FSO node, ρ be the radius of a transceiver, and θ be the divergence angle of a transceiver. We approximate an FSO transceiver's coverage area (which is the vertical projection of a lobe) as the combination of a triangle and a half circle. Let R be the height of the triangle, which means the radius of the half circle is $Rtan(\theta)$. Also, let τ be the length of the arc in between two neighboring transceivers on the 2-d circular FSO node.

Assuming that n transceivers are placed at equal distance gaps on the circular FSO node, and since the diameter of a transceiver is 2ρ :

$$\tau = \frac{2\pi r - 2n\rho}{n}$$

The angular difference between any two neighboring transceivers is given as:

$$\varphi = 360^0 \frac{\tau}{2\pi r}$$

Let L be the coverage area of a single transceiver, which can be derived as:

$$L = R^2 tan(\theta) + 0.5\pi(Rtan(\theta))^2$$

For the effective coverage area C of a single transceiver, two cases can happen based on the values of φ, θ, R, and r:

1. Coverage areas of the neighbor transceivers do not overlap

$$Rtan(\theta) \leq (R + r)tan(0.5\varphi)$$

   In this case, the effective coverage area is equivalent to the coverage area, i.e. $C = L$.

2. Coverage areas of the neighbor transceivers overlap

$$Rtan(\theta) > (R + r)tan(0.5\varphi)$$

   In this case, the effective coverage area is equivalent to the coverage area excluding the area that interferes with the neighbor transceiver. Let I be the interference area that overlaps with the neighbor transceiver's coverage, then $C = L - I$.

   Notice that the interference area I is not fully useful for communication, since the signal the transceiver receiving is garbled by the presence of the signal from the adjacent transceiver(s) due to interference, unless we use WDM for the adjacent transceivers. LOS can still be achieved by selecting one of the transceivers for communication, however the other transceiver(s) receiving signal will be useless until the communication is over from the FSO node in the area I. Therefore, we do not count the area I in the coverage area, though this does not mean that those interference areas are totally ineffective.

3.2.1.1 Calculation of the interference area I

As shown in Figure 3.4, the interference area I is composed of two isosceles triangles and two leftover pies. To find this area, the geometry for calculating the pieces of the area is needed. We need to find the angles x and y, and the length k, as shown in Figure 3.5. From Figure 3.5(a), we can write the following relationships:

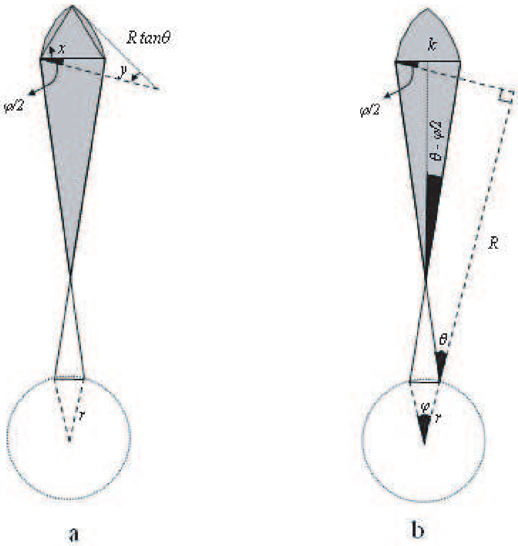

Figure 3.5: Calculating the area of interference between two adjacent transceivers

$$x + (0.5\varphi) = \frac{180 - y}{2}$$

$$\frac{k}{2cosx} = 2Rtan(\theta)sin(y/2)$$

$$k = 2\frac{R}{cos(\theta)}sin(\theta - \varphi/2) - 2rsin(\varphi/2)$$

Using x, y and k, the area of the upper isosceles triangle can be found.

3.2.1.2 Calculation of the maximum range R_{Max}

Another important unknown is the maximum range R_{Max} that can be reached by the 2-d FSO node. R_{Max} is dependent on the transmitter's source power P dBm, the receiver's sensitivity S dBm, the radius of the transmitter ρ cm, the radius of the receiver (on the other receiving FSO node) ς cm, the visibility V km, the optical signal wavelength λ nm, and the particle distribution constant q. FSO propagation is affected by both the atmospheric attenuation and the geometric spread , which practically necessitates the source power to be greater than the power lost [65].

Thus, for a conventional photo-detector (PD) sensitivity of S=-43dB, the following inequality must be satisfied for the PD to detect the optical signal:

$$S - P > A_L + A_G$$

$$-(P + 43) > A_L + A_G$$

Substituting A_L and A_G leads us to inequality, minimum solution of which is R_{Max}[65]:

$$-(P + 43) > 10log(e^{-\sigma R}) + 10log(\frac{\varsigma}{\rho + 50R\theta})^2$$

where

$$\rho = \frac{3.91}{V}(\frac{\lambda}{550nm})^{-q}$$

Note that the height of the triangle within the coverage area of a transceiver, R can be found by $R_{Max} = R + Rtan(\theta)$.

We optimize the total effective coverage area nC of the 2-d circular FSO node, though other metrics (such as ratio of uncovered area and total possible area) can also be chosen. In addition to P, θ, and V; the size of the FSO node (i.e. the radius of the FSO node circle r and the radius of a transceiver ρ) also plays a major role in the optimal number of transceivers n. Since C is dependent on P, θ , V and n; for given r and ρ, the optimization problem can be written as:

$$max_{\theta,P,V,N} nC(\theta, P, V, n)$$

such that

$$\theta \geq 0.1mRad$$

$$P \leq 32mW$$

$$V \leq 20KM$$

In our search for the best n, for a particular FSO node and transceiver size,

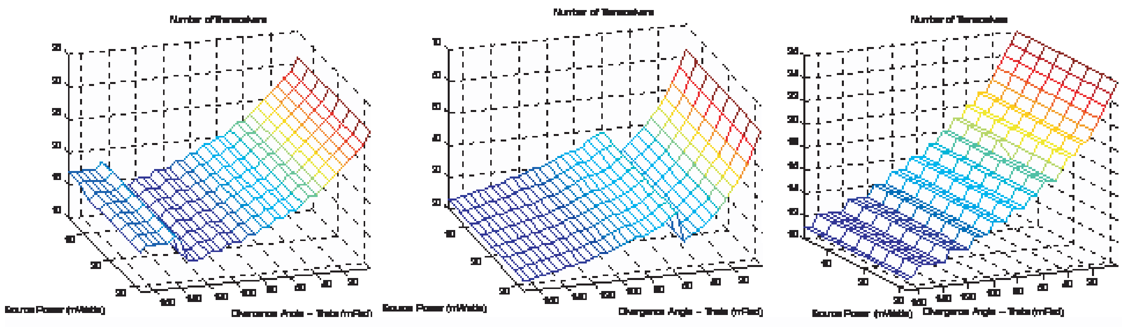

(a) r = 1cm, ρ=0.1cm **(b)** r = 20cm, ρ=1cm **(c)** r = 20cm, ρ=2.4cm

Figure 3.6: Number of Transceivers as a function of divergence angle and transmitted power

we varied P, θ, and V based on current FSO technology and literature [65]. We varied P from 4mW up to 32mW, as conventional lasers and LEDs use 4-10mW and 4-30mW respectively. Similarly, we varied θ from 0.1mRad up to 170mRad, as lasers and LEDs have 0.1-100mRad and 139-240mRad respectively. Also, we varied the radius of the circular FSO node from 1cm to 20cm, which includes very small FSO node sizes (1-5cm of radius) for indoor usage as well as large sizes (10-20cm of radius) for outdoor usage. Finally, given a circular FSO node radius r cm, we varied the transmitter (or transceiver) radius from 0.1cm to $r/8$. This means for large FSO nodes (e.g. r=20cm) transmitter radius can be more than 1cm, which is larger than current LED sizes. However, it is possible to approximate large transmitter sizes by using a mesh of LEDs and PDs instead of a single LED and PD. Therefore, we do not deem this as a problem.

Figure 3.6 shows the allowed number of transceivers on a spherical antenna for various sizes. Source power and visibility have no effect on the optimality of the number n of the transceivers on the FSO antenna. As TeX divergence of the light source is decreased, more and more transceivers can be packed on the antenna. Similarly Figure 3.7 shows that communication range is directly proportional to the source power and inversely proportional to the divergence angle.

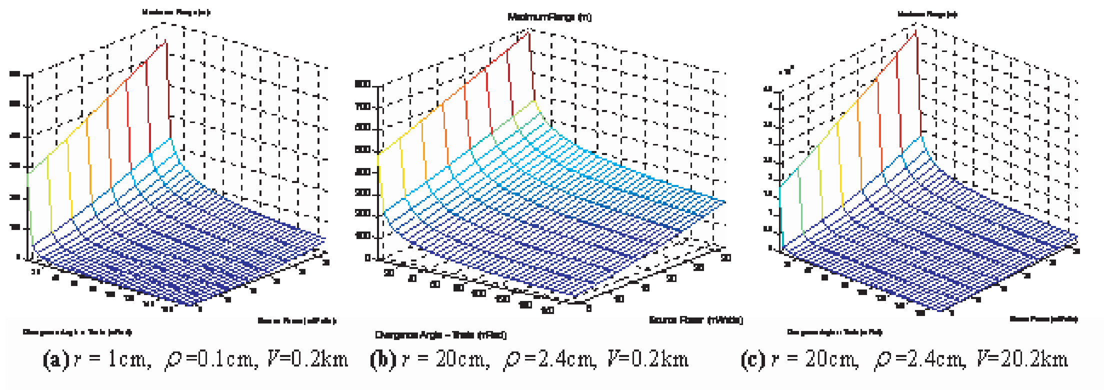

Figure 3.7: Maximum communication range

3.2.1.3 Design Recommendations

The value of the communication range, R_{Max}, for various FSO node designs is very important as it shows scalability of our circular 2-d FSO node designs for long distances. The maximum communication range of the node depends solely on the area of the transceiver (i.e. the radius ρ) for fixed θ and P. Depending on the size of the optical antenna for a specific weather condition, the node design may be optimal for either indoor or outdoor operation.

3.3 Auto-alignment Circuit

In this section we describe the design of the auto-alignment circuit. The basic functionality of the auto-alignment circuit is to monitor the incoming light beams at each transceiver and maintain continuous communication between two mobile optical antennas by dynamically latching appropriate transceivers within their LOS. Figure 3.8 shows the basic schematic of the circuit for one optical antenna. Figure 3.9 is the schematic for an antenna with four transceivers. In the event of misalignment, the circuit first (i) searches for an existing LOS between the two spheres, and then (ii) continues data communication through the new LOS, once a new LOS is established. These two functionalities are implemented in a common hardware for all the transceivers on a single spherical optical antenna.

The part of the circuit that monitors an existing LOS is shown as the "LOS Unit", which gives out a logical high output when an LOS is present between the two

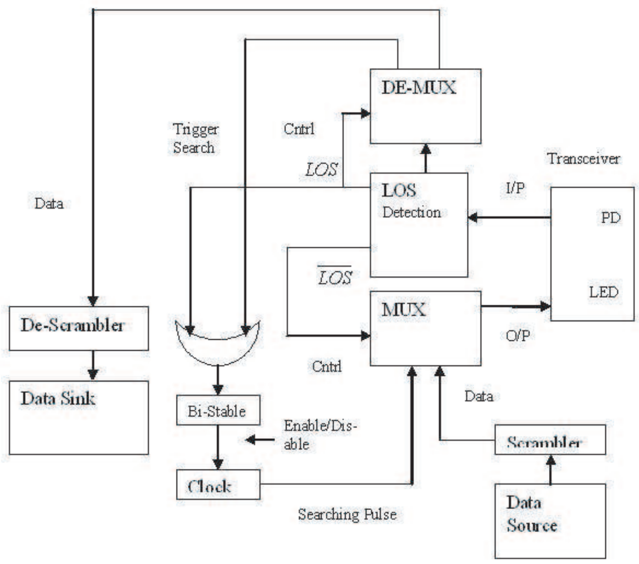

Figure 3.8: Schematic of the basic alignment circuit

communicating antennas and a logical low input when the LOS is lost. The logical low output triggers the "LOS searching". During this phase, data transmission is temporarily aborted and search pulses are sent out in all the directions looking for LOS. The second sphere, which now moved to a different location, also drops LOS and hence it too starts to initiate LOS searching. The spheres eventually receive the search pulses upon existence of a new LOS, which causes first a high output from the LOS Unit and then restoration of the data transmission. For cases when multiple channels are aligned, we used a priority decoder to select a channel via the LOS signals from each transceiver. When no channel is aligned, the system searches for alignment by sending pulses to each channel. As soon as one or more channels get aligned, it starts to send data signal out through the aligned channel. Thus, the logical data channel (or stream) is assigned to the physical channels dynamically depending on whether or not they are aligned.

3.4 Experiment illustrating Mobile FSO Communication

We performed a fun experiment to demonstrate the concept of spatial diversity and LOS auto-alignment in the case when multi-channels are aligned. We built one

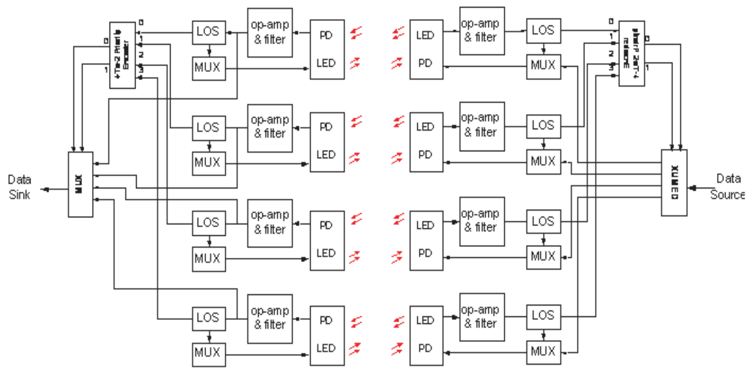

Figure 3.9: Alignment Circuit for four optical transceivers

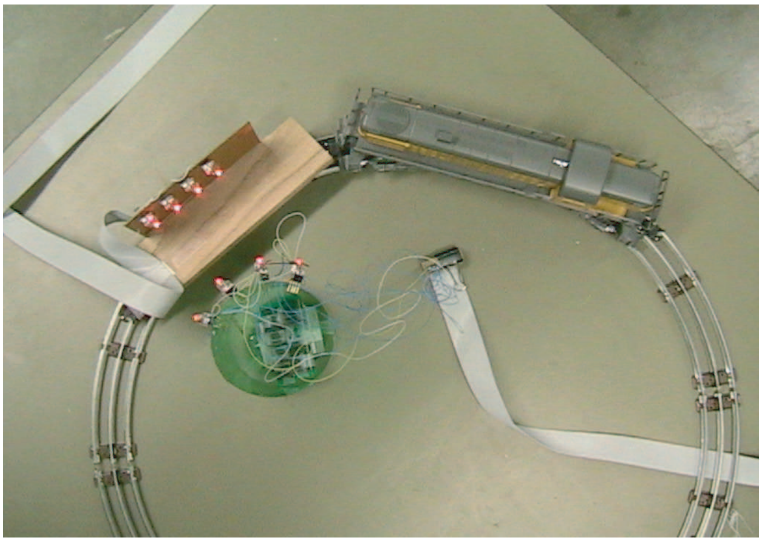

Figure 3.10: Pulses being sent out when there is no direct link present (No LOS)

cylindrical and one planar optical antenna with 4 duplex optical channels on each. Each optical transceiver included an LED with a divergence angle of 240 and a PD with field of view of 200. We spaced four transceivers on the cylindrical surface with an equal separation angle of 320 along a circumference normal to the cylinder axis. The planar surface also included four transceivers equally spaced along a line. We then placed the planar surface as part of train's cargo, and moved the train along a circular path of radius 30cm to create relative mobility. As the train moves the transceivers get aligned and misaligned.

Figure 3.10 shows a misalignment instance in which the search pulses are sent out by all transceivers and LEDs are glowing. Figure 3.11 shows an instance of

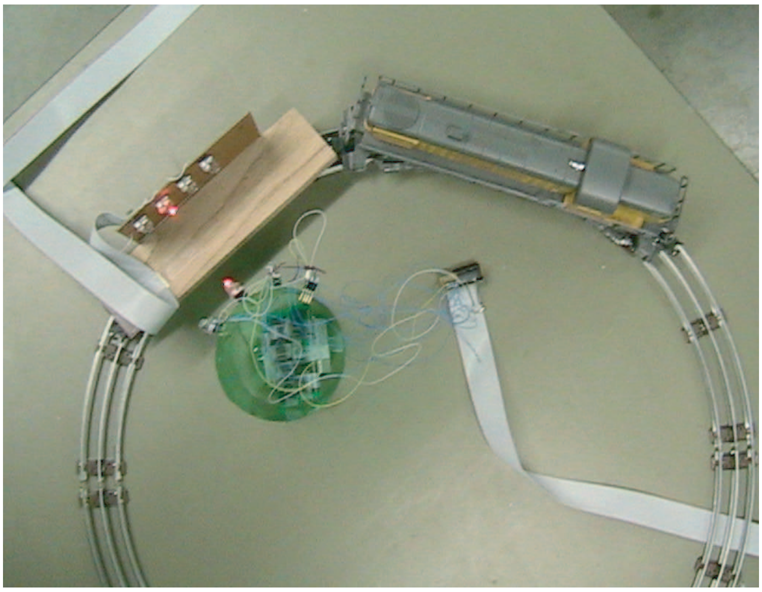

Figure 3.11: When an LOS is found, data is being transmitted

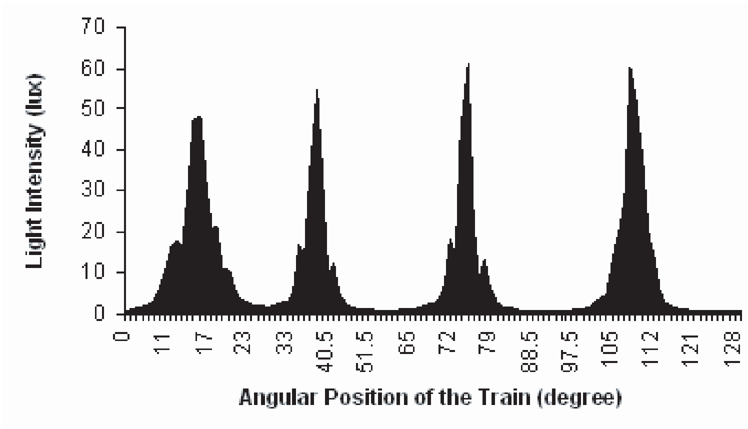

Figure 3.12: Intensity variation at the train as it moves around the circle

alignment in which two transceivers are in LOS with each other and data transmission is going through them. This pattern repeats as the train travels along the circular path as shown in Figure 3.12. Notice that, LOS periods can be increased by appropriately tuning the light intensity threshold at PDs, the divergence angles of LEDs, the field of view angles of PDs, and by increasing tessellation density. The speed of the circuit should be more than the speed of the relative movement between the spheres so as to maintain a smooth data flow.

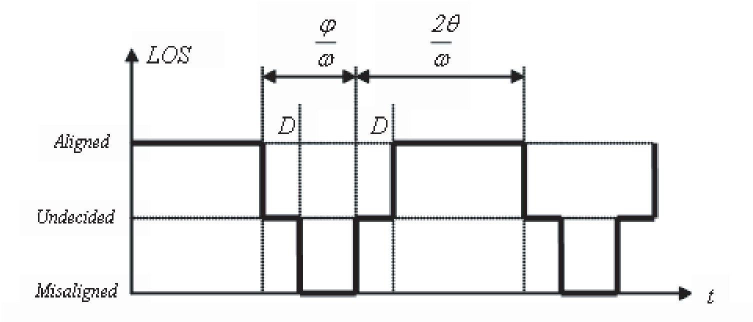

Figure 3.13: Intensity thresholds at the photo-detector corresponding to LOS alignment

3.4.1 Mobility Analysis

Here we analyze the above experiment in terms of the time for which the transmitter and receiver are aligned as a function of train's angular velocity and the response time (delay) of the alignment circuit. The various time factors and the corresponding intensity levels in the experiment are shown in Figure 3.13.

Consider a train moving with an angular speed of ω radians/s. Given the light intensity profile in Figure 3.12, we can draw a generic LOS plot as in Figure 3.13 for an LOS Detection Unit with a delay D seconds. Here, the length of alignment period will depend on LED's divergence angle θ and the train's speed; and the length of misalignment period will also depend on ω as well as density of tessellation which could be quantified as φ, the angle during which alignment is lost. Notice that both θ and φ depends on LED's optical characteristics as well as the distance between the train and the stationary cylindrical FSO node.

Interestingly, in terms of the overall percentage of time the two FSO nodes are aligned, t_A , the train's speed will only affect the performance depending on the circuit delay. This relationship could be characterized as:

$$t_A = \frac{2\theta - D\omega}{2\theta + \varphi}$$

To observe effects of the circuit delay and mobility, we have plotted t_A with respect to ω and D in Figure 3.14. We have chosen $\varphi = 0.5^0$ to see the behavior for a high density tessellation, and the divergence angle $\theta = 2^0$. Notice the increased effect of mobility in performance when circuit delay is higher. It is worth noting that

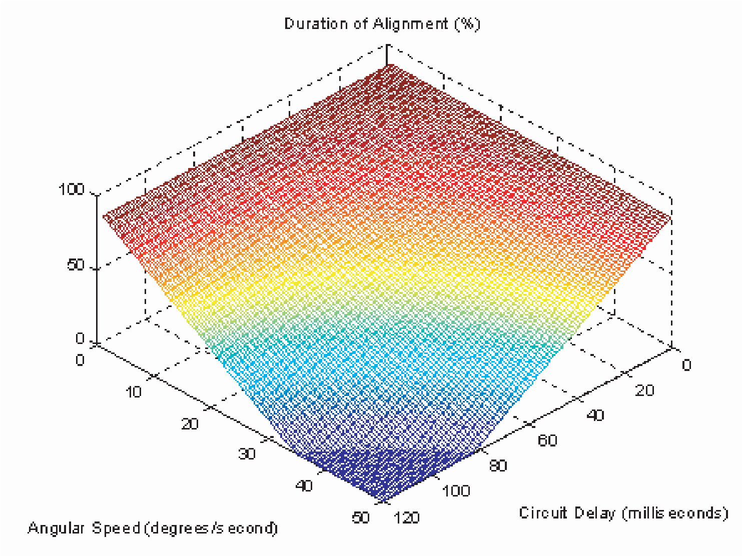

Figure 3.14: Duration of alignment with respect to the speed of the train and circuit delay

Transmitter Parameters	Receiver Parameters	Atmospheric Parameters	Link Parameters
Transmitted Power	Sensitivity	Visibility	Range
Divergence	Field of View	Wavelength	
Size	Size		
Transceiver Spacing	Transceiver Spacing		

Table 3.1: Parameters used for FSO simulation

very high mobility is tolerable for very realistic circuit delay ranges, e.g. 50 degrees/s for less than 10 milliseconds circuit delay. Given that our experimental circuit had a delay about 200ns, this result shows practicality of high-density tessellation of optical transceivers.

3.5 NS2 Simulation of FSO Optical Antennas

We also developed NS-2 simulation components to simulate FSO propagation and mobile FSO nodes. We modeled the line-of-sight recognition between the two nodes in 2-D in NS2. We also modeled the propagation of the light beam from an LED/VCSEL/Laser and its reception.

We simulate a 2-D circular FSO structure to validate our simulation components as well as to present proof-of-concept for possibility of applying spatial reuse and angular diversity for optical wireless access. Making use of our simulation components of FSO in NS-2, we have simulated a 2-D scenario on the XY-plane. In this 2-D configuration, we have a single mobile FSO node which circularly moves around four stationary FSO nodes. The stationary nodes are located in a circular pattern and are connected via wired links to a single central node. The combination of the central node and the stationary FSO nodes simulates an FSO device structure with spatial reuse of transceivers and angular diversity for LOS[1].

As the mobile node moves around the stationary nodes, an FTP session is alive between the central node and the mobile node. Initially, the experiment starts with the mobile node and one of the out stationary nodes in LOS. Soon after the session is established, the node moves around the stationary nodes at a constant rate of speed. For our experiments, all wired links are 100 Mbps with 2ms delays and Drop Tail queues, while the FSO nodes are configured to only transmit at 20 Mbps. Routing is performed by ad hoc DSDV routing agents and MAC is facilitated by 802.11 that is already present in NS-2.

From the plots in Figure 3.15 we can see that, using the spherical antenna structure, it is possible to achieve connectivity between mobile nodes even with a very small number of transceivers. The experiments were configured in such a manner that LOS is not always present, thus showing that connectivity is reestablished when the nodes are back in LOS. This is demonstrated by the plateaus in the TCP sequence number graph. Furthermore, increase in the TCP sequence numbers imply that (i) all simulation components from physical layer to transport layer are setup properly, thereby provides validity of our simulation building blocks, and (ii) transport level goodput can be achieved over a highly variant (i.e. frequent LOS changes) FSO environment.

3.6 Future Work

We demonstrated connectivity between two mobile FSO antennas by using our auto-alignment circuit. The connectivity is intermittent and loss prone at this

[1]Later, we implemented multiple interfaces over a single mobile node to simulate multiple transceivers on a node, which is more accurate modeling of the spherical FSO antenna

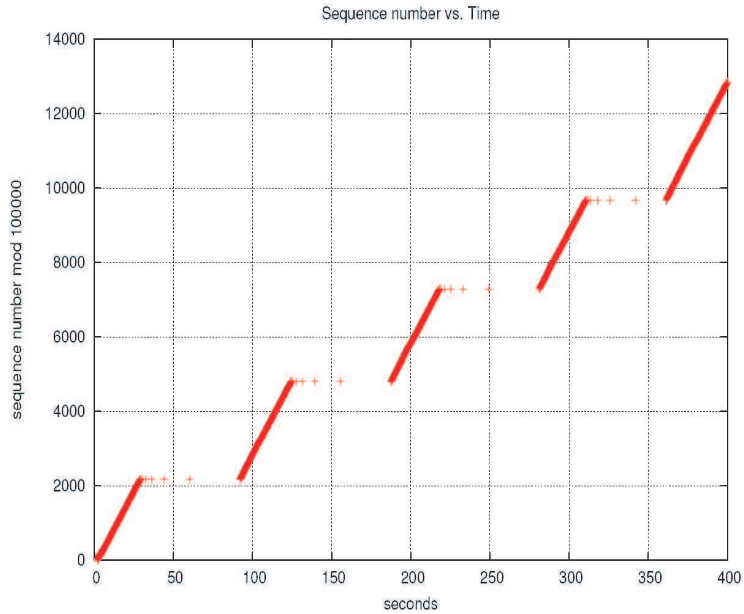

Figure 3.15: TCP sequence numbers as the nodes move

point of time. To improve the reliability of such a connection, we need to come up with optimal hand-off protocols between the transceivers. To maintain connectivity between mobile nodes with no or little loss of information, we need to design smart buffers that can handle intermittent loss of connectivity. Also, by using suitable forward error correction codes, we can further improve the quality of such mobile communication.

For the near future, we want to implement our localization scheme and name-to-address mapping on the spherical antennas. By using existing routing protocols like GPSR, we will evaluate perforce of our localization frame work in stationary and mobile situations.

CHAPTER 4
2-Dimensional Arrays for FSO communication

4.1 Introduction

The use of multiple element antennas to increase the capacity of a communication channel is well known. It has been demonstrated that capacity can be increased linearly as a function of the number of antennas in wireless communications [13], [12], [14]. However, traditionally, free-space optical (FSO) communications use a single transmitting antenna (laser/VCSEL/LED) and a single receiving antenna (a photo-detector) for single channel communication [65].

Multi-element array design for FSO communication is very attractive since it offers high aggregate bandwidth and link robustness due to spatial diversity. As an example, optical transceivers are capable of operating at bandwidths greater than 100 Mbps. With each transceiver operating at a speed of 100 Mbps, a 10×10 array will give 10 Gbps in aggregate capacity. On the other hand, close packaging of transceivers on the arrays is not possible without avoiding interference of optical beams for neighboring transceiver elements. The main issues of multi-channel operation are interference (or cross-talk) between adjacent channels due to finite divergence of the light beam, and misalignment of the array elements due to mechanical vibration.

In this chapter we examine the feasibility of using 2-dimensional multiple element array antennas for free-space optical communications. Spatial diversity due to multiple antennas on 2-d arrays can increase aggregate link bandwidth. On the other hand, simultaneous transmissions between the elements on the arrays can cause inter-channel interference, reducing the effective bandwidth. We model this inter-channel interference as noise and find the probability of error due to such noise. Based on this error model, we then derive channel capacity estimations. We introduce a new metric "Bandwidth-Volume product" analogous to optical fiber's "Distance-Bandwidth" metric to gauge the performance of such arrays. We present design guidelines based on the link range, number of optical transceivers (elements)

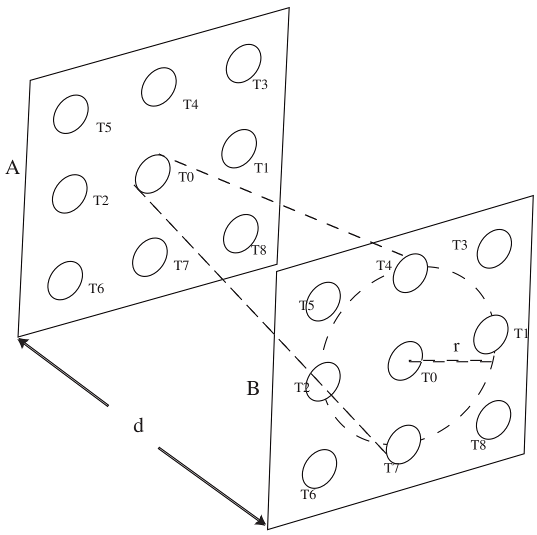

Figure 4.1: Proposed array design for FSO communication.

that can be packed on a given array, and the achievable aggregate bandwidth. We focus on inter-channel interference issues and present an analysis on the behavior of the aggregate bandwidth as a function of such interference for rectangular arrays. The results are equally applicable to circular arrays and other forms of 2-dimensional arrays.

4.2 Array Description

The 2-dimensional array we propose FSO communications is shown in Figure 4.1. The circles denote the optical transceivers, i.e. a light source (Laser/LED) and a photo-detector. Multiple such transceivers are spaced on the array. The total number of transceivers per unit area on an array is referred to as *package density* ρ.

Two such identical arrays face each other to facilitate communication between the corresponding optical transceivers on the arrays. In such a scenario, ideally each of the transceivers on the array is supposed to communicate *only* with the corresponding transceiver on the opposite array. But because of the finite transceiver angle, the light signals transmitted will diverge by the time they reach the opposite array and they are not only received by the corresponding transceiver on the opposite array, but also by its neighboring transceivers, causing interference.

For example, as shown in Figure 4.1, consider the transmission from the transceiver T_0 on the array A, T_0^A to T_0 on the array B, T_0^B. For a transmission between the transceivers AT_0 and BT_0, as shown in the figure, the cone from the transceiver AT_0 extending onto the array B defines the field of view of the transceiver. The radius of the cone on the array B is a function of the distance between the two arrays d and the transceiver angle θ as given by:

$$r = dtan(\theta)$$

Because of the finite transceiver angle θ, not only T_0^B is present in T_0^A's field of view, but also four more transceivers T_1^B, T_2^B, T_4^B, and T_7^B. Extending the argument, T_0^B not only receives light from T_0^A, but from all the transceivers in whose field of view T_0^B exists. We call those transceivers as "potential interferers".

Interference at T_0^B can happen if the intensity of light coming from these potential interferers is greater than I_T. Since the intensity of the light beam varies across its cross section, not all the potential interferers can cause cross talk due to their transmissions. Cross talk is caused only when these interferes at a distance "Y" from T_0^A such that

$$I_Y \geq I_T$$

If there are $N \geq 1$ interferers at distance "Y", crosstalk occurs if

$$NI_Y \geq I_T$$

Let us define a distance on the array Y_T, such that

$$I_{Y_T} = I_T$$

So transceivers spaced within $2Y_T$ (one Y_T for each of the adjacent transceivers) are bound to interfere with each other resulting in crosstalk. So the minimum separation between the transceivers on the array should be greater than twice Y_T, so adjacent simultaneous transmissions does not result in crosstalk. Numerically, for arrays at a distance of 100 meters, and with a transceiver angle of θ as 1 mrad, the value of Y_T lies around 40 cms if I_T is set to $\frac{1}{2}I_o$, where I_o is the intensity at the

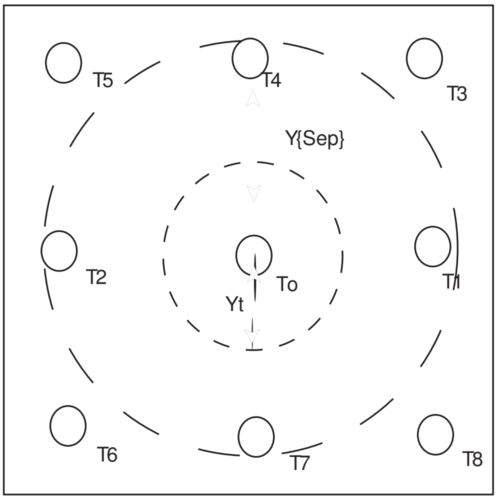

Figure 4.2: The circles with radii Y_T and Y_{Sep} on the array.

center of the laser beam. This suggests that we cannot place the optical transceivers closely packed in a small area on a compact array, even though with current day technology, we can obtain miniature lasers and photo-detectors.

4.3 Interference Model

In a single channel FSO communication system, the received signal quality is limited by Gaussian shot noise following the photo-detector [68]. However, in a multi-channel system like in an array, noise is a combination of the above described AWGN and noise caused by inter-channel interference. Since the AWGN noise is common to all the receivers and can be combated either by increasing the signal power or by using error control codes, the noise contributed only by the inter-channel interference is considered in the remainder of the chapter for discussion. In this section, the resulting error due to such noise the its effect on the channel capacity is discussed.

Let us define a packaging density of the transceivers on the array ρ_o that satisfies the minimum spacing ($2Y_T$) condition to avoid inter-channel interference.

$$\pi {Y_T}^2 \rho_o = 1$$

and for an arbitrary spacing Y_{Sep}

$$\pi {Y_{Sep}}^2 \rho_o \leq N_o$$

$$N_o I_{Y_{Sep}} \leq I_T$$

Interference happens when the package density ρ is greater than the optimal density ρ_o. The total number of transceivers N for a package density ρ within the field of view θ(r) is given by:

$$\begin{aligned} N &= \pi \rho r^2 \\ &= \pi \rho (d tan \theta)^2 \end{aligned} \tag{4.1}$$

The total number of interferers is $N-1$, as N includes AT_0. These $N-1$ transceivers could have been placed anywhere on the array with in a radial distance of r from AT_0. Interference can happen when a subset of these transceivers transmit at the same time as T_0^A. The probability of that event gives the probability of error resulting due to interference. That is obtained in the following discussion.

Let us assume that these $N-1$ transceivers are distributed to be on J imaginary circles of radii r_J. We can calculate the error probability due to interference in terms of each of the J circles as one unit.

The number J is decided by the Y_{Sep} of the array.

$$J = \left\lfloor \frac{r}{Y_{Sep}} \right\rfloor$$

Since the transceivers are uniformly spaced distances Y_{Sep}, the radius of the Jth circle is $r_J = J \cdot Y_{Sep}$. The number of transceivers K_J on the Jth circle is a function of package density ρ of the transceivers on the array. This is given by:

$$K_J = \pi \rho (r_J)^2 - K_{J-1}$$

$$K_o = 1$$

Interference at T_0^B happens only when $K_J > N_o$ and $K_j I_{jY_{Sep}} \geq I_T$, for $j = 1, 2..J$. To understand when exactly interference happens, consider the following cases, for $j = 1, 2, ..J$.

1. T_0^A transmits a 1 and K_j a 1
2. T_0^A transmits a 1 and K_j a 0
3. T_0^A transmits a 0 and K_j a 1
4. T_0^A transmits a 0 and K_j a 0

Interference happens only in $Case3$, since only then T_0^B receives a false threshold at its receiver. In all other cases the received light intensity does not cause a false threshold. The probability of error P_e caused by such an event can be expressed as: *the probability that all the K_J transceivers on at least one of the J circles is transmitting a ONE when T_0^A is transmitting a ZERO.*

To formulate P_e, we start with expressing the probability that a transceiver not transmitting a *ONE* as p_0. For a circle j with K_j transceivers, the probability that the circle is not transmitting a *ONE* can be expressed as:

$$P_{j,0} = {p_0}^{K_j}$$

Similarly, the probability that none of the J circles is transmitting a *ONE* can be written as:

$$P_{J,0} = \pi_{j=1}^{J} P_{j,0}$$

Based on this notation, P_e could be written as:

$$\begin{aligned} P_e &= \left[1 - P_{J,0}\right] p_0 \\ &= \left[1 - \pi_{j=1}^{J} {p_0}^{K_j}\right] p_0 \end{aligned} \tag{4.2}$$

We assume equal transmission probability for a *ONE* and *ZERO* ($p_0 = 1/2$).

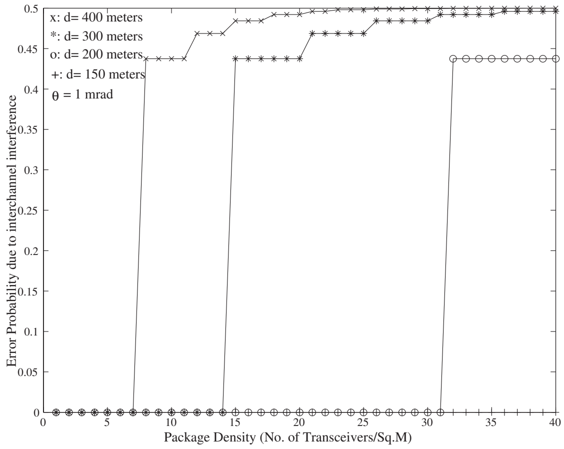

Figure 4.3: Error probability variation with package density for various distances.

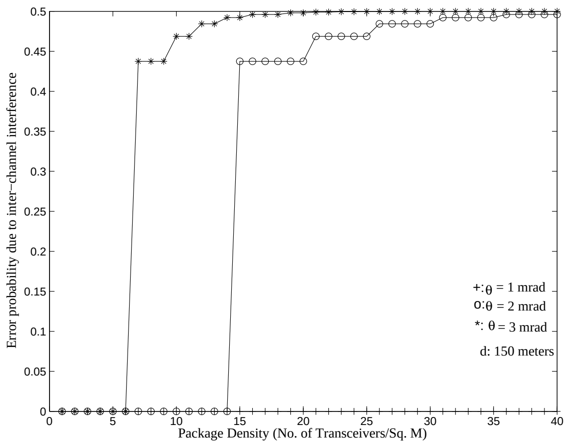

Figure 4.4: Error probability variation with package density for various divergence angles.

As it can be seen from (4.2) and the derivation of K_j, the error probability is a function of the package density ρ, the distance between the arrays d and the transceiver angle θ. Figure 4.3 and Figure 4.4 show the variation of P_e with d and θ as a function of the package density on the array ρ.

4.4 Aggregate Channel Capacity for the Array Transmission

Use of arrays for FSO communication gives the benefit of higher transmission bandwidth due to spatial diversity. Higher package density has a potential

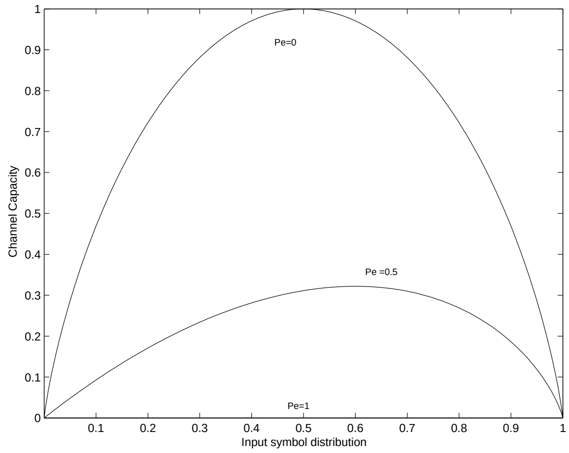

Figure 4.5: Capacity of the binary asymmetric channel for the array antennas.

for higher aggregate bandwidths, but at the same time causes inter-channel interference. In this section, we look into the question: How is the aggregate channel capacity effected by the error probability due to interference?. We model the array communication channel as a Binary Asymmetric Channel and find the relationship between the capacity of such a channel to the package density of an array.

As described in Section 4.3, an error in the reception occurs only when T_0^A transmits a *ZERO* and at least one of the interfering circles transmits a *ONE*. Since the error is caused asymmetrically, each channel on the array corrupted by inter-channel interference (cross-talk) can be modeled as a Binary Asymmetric Channel. The capacity of such a channel is known to be:

$$C = max_{p_1} H(\bar{p_1}\bar{P_e}) - p_1 H(\bar{P_e})$$

where C is the channel capacity, p_1 is the input symbol (*ONE* or *ZERO*) probability distribution, and P_e is the probability of error. A plot of the capacity C versus the input distribution is shown in Figure 4.5 for various error probabilities.

P_e for the array communication system is given by Equation 4.2. By fixing a specific operating point on the capacity curve for the arrays, we fix the error probability P_e and in turn a package density, divergence angle and link range.

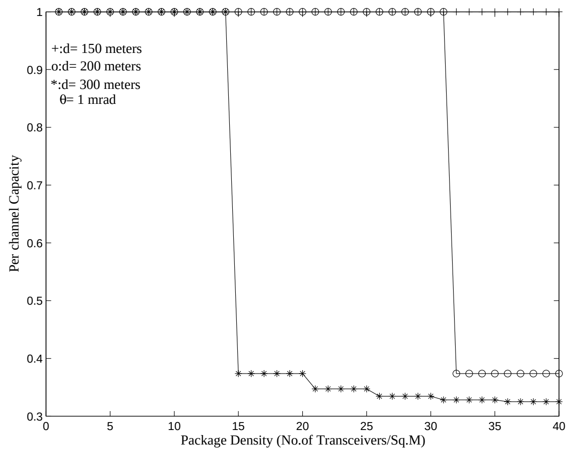

Figure 4.6: BAC capacity variation with array package density for various distances.

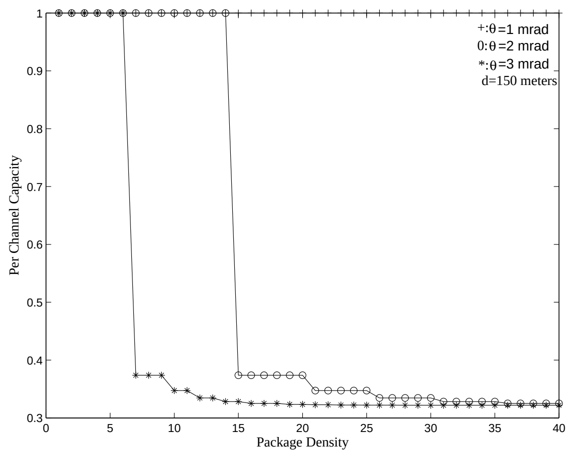

Figure 4.7: Channel capacity versus Package density with divergence angle.

4.5 Design Guidelines

In Figure 4.6 and in Figure 4.7 the variation of per-channel capacity with package density is illustrated. As the package density increases, the error probability increases and hence the capacity decreases. The specific package density at which the capacity drops from 1 is a function of the distance between the arrays, and the angle of the transceivers and the specific arrangement of the transceivers on the array. The figures demonstrate the behavior of the capacity for a uniformly spaced transceiver configuration.

We can choose the package density such that each channels operates at a full capacity. Alternatively, we choose a package density wherein each channel operates at a lower capacity point and gets a higher aggregate bandwidth due to multiple operating channels. For example, we can choose an array with 5 transceivers, each operating at 100 Mbps each, with an aggregate bandwidth of 0.5 Gbps. Alternatively, we can pack 10 transceivers, each operating at $\frac{3}{4}$'s of its capacity, but with an aggregate bandwidth of 0.75 Gbps. For example as shown in Figure 4.6, 25 transceivers operating at 0.35^{th} of the capacity offer a higher aggregate bandwidth than 20 transceivers operating at 0.375^{th} of the capacity.

4.6 Bandwidth-Volume Product (BVP)

We define the performance of an FSO communication channel by three design parameters: (i) number of channels per array, (ii) the capacity of each of the channel in bits per second, and (iii) the distance over which the arrays can communicate with that capacity. We define a useful design metric that incorporates all the above parameters of the system as a product. We designate it as *Bandwidth Volume Product (BVP)*. "Bandwidth" denotes the capacity of a single channel, i.e. the unit of Bandwidth is *Mbps*. "Volume" describes the 2-dimensional nature of the array and the distance over which they can communicate. So, the Volume is simply multiplication of the number of channels on the array and the communication distance, i.e. the unit of the Volume here is *meter*. This means unit of BVP is Mbps-meter.

BVP is analogous to the "Bandwidth-Distance Product" metric of a fiber-optic link. In the case of a fiber-optic link, it is the fiber dispersion that adversely effects the aggregate capacity, whereas in the multi-channel FSO link, it is the interference.

The advantage of BVP is that it provides an integrated performance evaluation measure to aid the decision process for choosing various parameters (e.g. d, θ) of the multi-element FSO system. The distance of operation, number of channels should be carefully chosen to achieve the desired capacity. Even if each of the channel is not operated at full capacity, one can still achieve high bit rates due to the presence of multiple simultaneous transmissions.

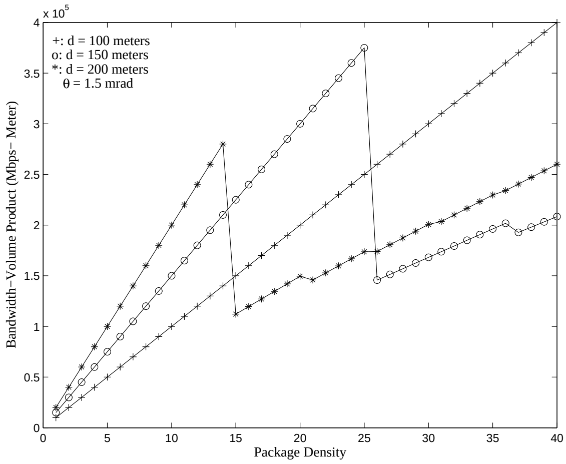

Figure 4.8: Bandwidth-volume product (BVP) versus Packaging density with Link Range.

4.7 Future Directions

We demonstrated that 2 dimensional arrays provide excellent bandwidths over short range communication links. To use these arrays over very long distances outdoors, very narrow beams coupled with auto-aligning mechanisms are needed to reduce inter-channel interference. Interference can also be decreased by using time multiplexing and coding techniques, thereby improving the performance. Also, we can use multiple wavelengths and filters to reduce interference, which again is another interesting research direction to improve performance of multi-element FSO systems.

The specific issues we ar going to undertake to improve the results and add new contributions are:

- Include the Gaussian noise in the interference model, to remove the ambiguity in computing the noise:

  In the noise computation, only the inter-channel interference is considered, as Gaussian noise effects equally all the channels. Inclusion of Gaussian noise makes the model more complete, but may not add any additional insight on the array performance in terms of its parameters.

- Coming up with an FEC scheme that exploits the "space" on the array:

The multiple channels in the array can be used to add redundancy to the communication link to improve its reliability. Unlike MIMO, channels on the FSO array are highly correlated as they are spatially close to each other. Because of this, there is no “diversity gain”. The possible design choices are to stagger the data streams in time and space, or provide link protection just by sending duplicate data steams etc.

CHAPTER 5
Error Analysis of Multi-Hop Free-Space Optical Communication

5.1 Introduction

The most important road block FSO facing to be accepted as a general purpose communication technology is drastic degradation of link quality during moderate to heavy fog and other adverse atmospheric conditions. The challenge is to increase the link reliability and make the link availability to meet industry's five-nine's [8] standard. Towards this, two important methods have been proposed in the literature [1], [17]. One is to provide hybrid link protection using an RF link, and the other is scaling the hop length down between the transmitter and receiver using multi-hop routing. This chapter focuses on the second approach, increasing the FSO link reliability by using smaller, multiple hops.

We focus on the channel error characteristics and analyze the error performance of Free-Space Optical (FSO) communication over multiple hops. We first develop an error model for a single hop based on visibility, atmospheric attenuation, and geometric spread of the light beam. We model atmospheric visibility by Gaussian distributions with mean and variance values to reflect clear and adverse weather conditions. Based on this, we find the end-to-end bit error distribution of the FSO link for single hop and multi-hop scenarios.

We present simulation results for decoded relaying, where each hop decodes the signal before retransmitting. We demonstrate that multi-hop FSO communication achieves a significant reduction in the mean bit error rate and also reduces the variance of the bit error rate. We argue that by lowering mean error and error variance, multi-hop operation facilitates an efficient system design and improves the reliability of the FSO link by application of specific coding schemes (such as Forward Error Correction techniques).

We present the error behavior due to atmospheric and geometric attenuation of the FSO signal for both single hop and multiple hop cases. We show that multiple hops enhance the reliability of the FSO link in both clear weather and bad weather conditions by reducing the mean and variance of end-to-end error. Since the mean and the variance of the error is reduced, we can design efficient error control codes to operate with FSO links. With this approach, we argue that FSO links can be made sufficiently reliable to be considered for last mile and metropolitan networks.

We model the multi-hop FSO communication system with a source terminal and a receiving terminal at the two ends, and a fixed number of intermediate relaying terminals. Each of the intermediate relaying terminals may either have the ability to decode the received signal or just amplify it before retransmitting. Since the FSO channel is slowly varying, we assume the attenuation experienced by a single bit to be a constant during its transit. The attenuation and error behavior for the individual hops is assumed to be independent.

We model the atmospheric visibility as a Gaussian random variable. We find the end-to-end error distribution for single hop and multiple hop cases, taking into account the effect of hop length and number of hops. Visibility for the clear weather and bad weather cases is modeled using different mean and variance values.

Errors on an FSO link can be modeled as *random errors* caused by attenuation and reduced signal-to-noise ratio (SNR) due to bad visibility conditions like rain, snow, and fog, and *burst errors* due to occasional obstructions and cloud-bursts. In this chapter we discuss the random errors caused by attenuation on the FSO channel. During clear weather conditions the FSO link has very low Bit Error Rate (BER), almost acting as a wired link. However, during adverse weather conditions, the BER due to random errors can be very high due to drastically reduced SNR. We propose two design metrics to evaluate the performance enhancements due to multiple hops. The first metric measures the reduction in the magnitude of the average BER by the use of multiple hops. The second metric captures the reduction in the variance of the error in the multiple hop case compared to single hop.

The rest of the chapter is organized as follows: In Section 5.2, we describe how the optical signal undergoes attenuation due to geometric spread, and atmospheric absorption and scattering. In Section 5.3 we present the error behavior of an FSO link over a single hop. In Section 5.4, we use simulation to analyze the error accumulation and distribution over multiple hops, and compare it with single hop with decoded relaying. In Section 5.5 we briefly introduce multi-hop systems with only amplified relaying. We conclude the chapter in Section 4.7 with directions for future work.

5.2 Signal Attenuation in FSO

FSO signal is subjected to two types of attenuation. The transmitted signal x is subjected to attenuation due to geometric spread, and the suspended particles in the atmosphere at various weather conditions [65]. One is fixed and the second is random.

5.2.1 Geometric Attenuation

In an FSO communication system, the geometric spread is a fixed function of the specific design parameters of the system and is given by [65]:

$$a_G = \frac{SA_R}{SA_T + \frac{\pi}{4}(\theta R)^2}$$

where SA_R is the area of the receiver, SA_T is the area of the transmitter, θ is the angular divergence of the light source, and R is the distance between the transmitter and the receiver.

5.2.2 Atmospheric Attenuation

The atmospheric attenuation is a time varying factor, which depends essentially on the visibility between the sender and receiver at the instant when the packet is being transmitted. It is given by [65]:

$$a_A(t) = e^{-\rho R}$$

where

$$\rho = \frac{3.91}{V(t)}(\frac{\lambda}{550nm})^{-q}$$

where $V(t)$ is the atmospheric visibility at a given time t, λ is the wavelength of the optical signal used, and q is the size of the suspended particles in the signal transmission path [65]. Turbulence in the atmosphere also causes errors due to distortion in the signal.

Over a single hop, the output signal at the receiver can be written as

$$y = a(t)x + n$$

where, y is the signal received and $a(t)$ is the attenuation as a function of time t, experienced by the input signal x. n is the additive white Gaussian noise (AWN) caused by the receiver circuit [68]. The total attenuation due to atmospheric propagation and geometric spread can be expressed as:

$$a(t) = a_G \cdot a_A(t)$$

where a_G is the attenuation due to geometric spread and a_A is the attenuation due to atmospheric propagation. The attenuation experienced by the signal causes random errors at the receiver due to reduced Signal to Noise Ratio (SNR).

5.3 Error Analysis of a Single hop FSO channel

A single hop FSO link can be modeled as a Binary Symmetric Channel (BSC) with an error probability P_e. The probability of error for such a channel with on-off keying is given by [15]:

$$P_e = Q(a(t)\sqrt{SNR})$$

where Q is the error function. Since the attenuation $a(t)$ is a function of the visibility, P_e, and hence the BER is a function of visibility. Since we assume a gaussian model for atmospheric visibility we obtain the distribution of P_e and hence for BER for each hop as shown in Figure 5.1.

Figure 5.2 illustrates the variation of the BER with SNR for different visibilities. As the visibility becomes worse, the received SNR decreases and the probability of error increases. An FSO system designed to work with a single visibility, and hence a fixed received SNR performs worse as the weather degrades. The channel

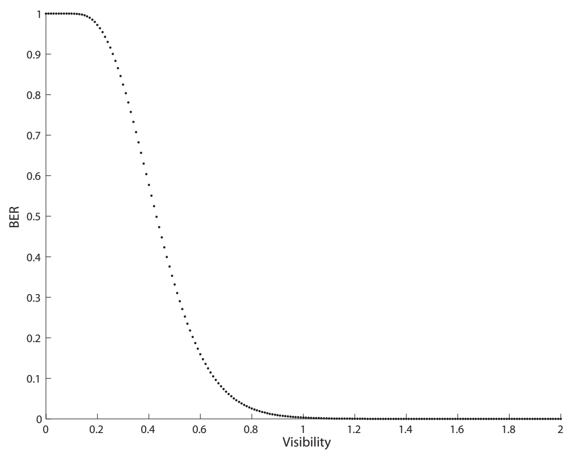

Figure 5.1: BER variation per hop with visibility.

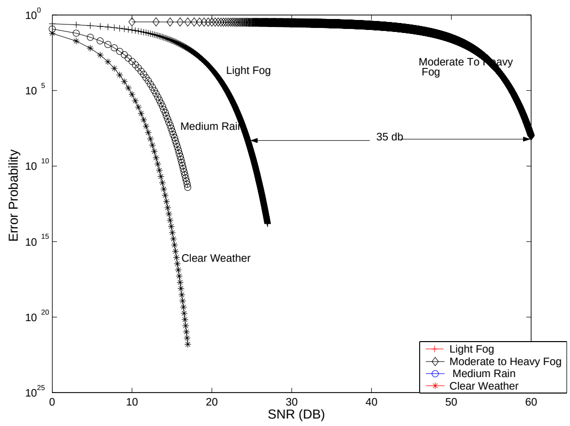

Figure 5.2: Error probability over a single hop with SNR for different visibilities.

behavior is worst for foggy conditions in the case of FSO communications.

The strategy to combat the degrading behavior due to decreasing visibility is either to have an adaptive strategy to increase the transmitted power keeping the SNR fixed as the weather degrades, or always leave a fixed power margin so as to work for a broad range of visibilities. The first method even though is more energy efficient than the second, is hard to achieve in reality, as it demands the channel state information time to time. We propose the use of multiple hops to minimize the error and also reduce its variance. By reducing the variance, we can design an FSO system that can be reliable for a wide range of channel conditions more efficiently.

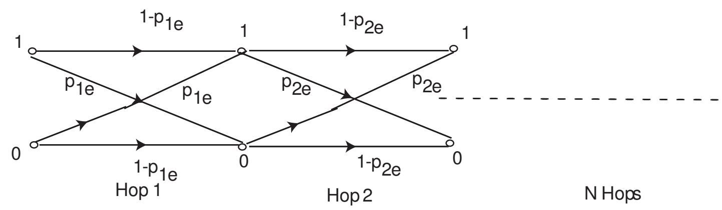

Figure 5.3: Multi-hop equivalent channel model.

5.4 Multi-Hop System: Decoded Relaying

The multi-hop FSO channel with N hops is modeled as a concatenation of N BSCs. It is illustrated in Figure 5.3. Since each channel is assumed to be independent, the end-to-end error probability and hence the BER for the multi-hop channel over N hops is given by:

$$P_{e(multi-hop)} = 1 - ((1 - p_1)(1 - p_2)....(1 - p_N))$$

Assuming that each of the crossover error probabilities of the BSC are on the order of 10^{-2}, the above expression is approximated for the clear weather conditions as:

$$P_{e(multi-hop)} = \Sigma_i^N p_i$$

We use this approximation for the simulation of end-to-end error accumulation over multiple hops in clear weather conditions.

In the case of decoded relaying, the multi-hop channel corresponds to the case where each intermediate terminal decodes the received signal and re-encodes before retransmission. This system does not propagate noise, as at each hop, the signal is reconstructed with a finite decoding error. At each stage there is also a delay which is accumulated over the total number of hops. For a given end-to-end length, the system can be operated as a single hop, or can be divided into multiple hops. The relationship between the number of hops and the error rate helps to determine how many hops have to be implemented. From Figure 5.4 we can get an estimate of how

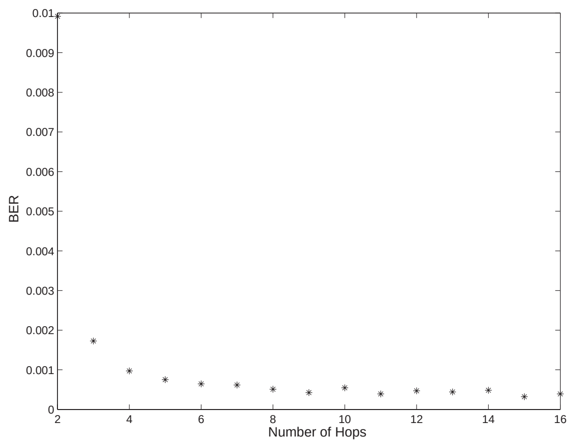

Figure 5.4: BER versus number of hops for a fixed link length.

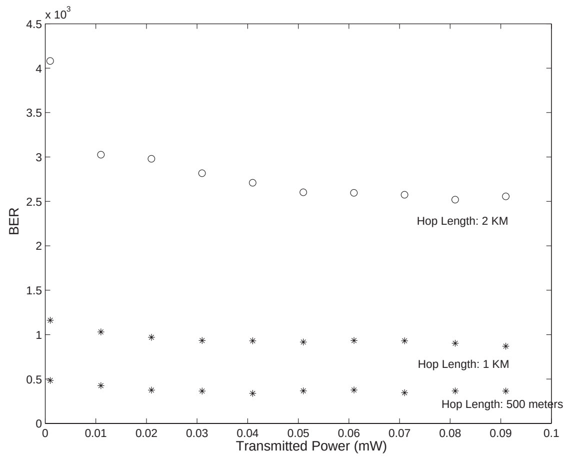

Figure 5.5: Transmitted power versus hop length.

many hops are optimal for desired operation. As seen, the decrease in the error is not significant after 8 hops for the given visibility distribution and the end-to-end link length.

The effect of hop length on the transmitted power and the resulting error rate can be seen from Figure 5.5. For the same transmitted power, the resulting error rate decreases as the hop length decreases.

Figure 5.6 shows how error gets accumulated over multiple hops as the hop length is increased. The error remains low till a hop length value of 500 meters and starts to build rapidly after that. Using this result, we fixed our hop length at 500 meters to simulate multi-hop error behavior.

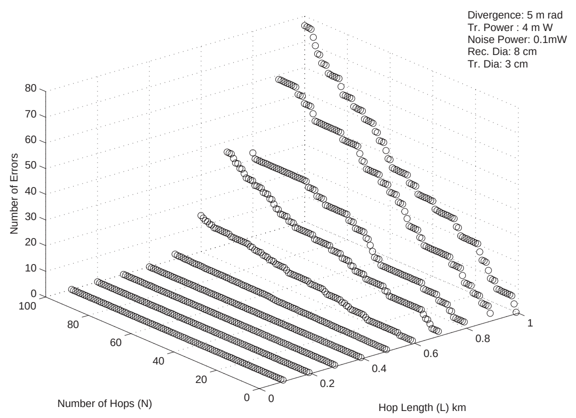

Figure 5.6: Error accumulation with hop length.

In the next two subsections, we find the error distribution over single hop and multi-hop scenarios for clear weather conditions and adverse weather conditions.

5.4.1 Clear Weather Conditions

For the case of clear weather, the visibility is taken as a Gaussian with a mean at 10 KM and a variance of 3 Km, representing clear weather to light rain conditions [34].The simulation results for both the single hop case and multiple hop case are presented. An end-to-end range of 2.5 KM is chosen for the FSO link. In the case of a single hop, the distance between the transmitter and the receiver is 2.5 KM. In the case of multiple hops, the range is divided into 5 hops, each hop being 500 meters. The end-to-end power used for both the cases is set to be equal. The end-to-end error distribution for a single hop case is shown in Figure 5.7(a) and for a multi-hop case is shown in Figure 5.7(b). The mean BER of the single hop is more than that of multi-hop. The error in the case of single hop is more widely distributed than in the case of a multi-hop. (For specific values, please refer to Table 5.1.)

5.4.2 Adverse Weather Conditions

For adverse weather conditions, the visibility is taken as a Gaussian with a mean at 3 KM and a variance of 1.5 Km, representing moderate to heavy rain/snow and light fog conditions [34]. The end-to-end range is 2.5 Km for a single hop and 5 hops with hop length of 500 meters in the case of multi-hop scenario. The end-to-

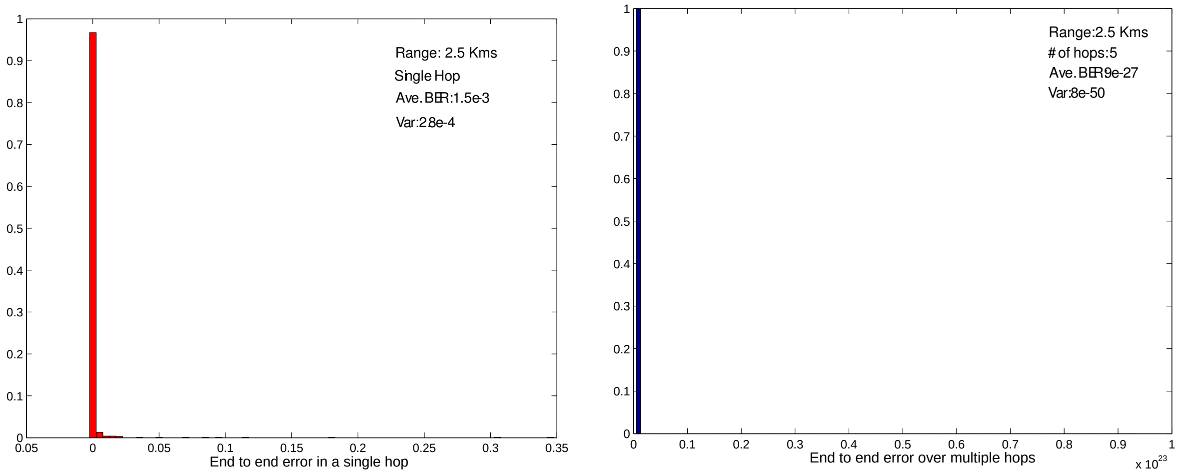

(a) (b)

Figure 5.7: Error distribution for clear weather conditions: (a) Single hop FSO link (b) Multi-hop FSO link.

Number of hops	Clear Weather Mean BER	Adverse Weather Mean BER	Clear Weather BER Variance	Adverse Weather BER Variance
1	1.5e-3	0.27	0.02	0.1176
5	9e-27	5e-3	8e-50	4.5e-3

Table 5.1: Comparison of mean BER and BER variance for Single Hop and Multi-Hop scenarios.

end error distribution for single hop scenario is illustrated in Figure 5.8(a). As seen the error is widely distributed causing the variance to be very high. Designing such an FSO link to operate reliably over wide range of visibilities is a challenge and also inefficient.

Figure 5.8(b) illustrates the end-to-end error distribution in the case of multi-hop operation. The error is contained within a small region, making the variance considerably small. The reliability of such an FSO link can be increased easily and efficiently compared to the single hop case.

Clearly, there is an improvement in both the mean and the variance in the case of multiple hops. A comparison of the mean error and the variance for both the single hop and multi-hop cases is given in the Table 5.1.

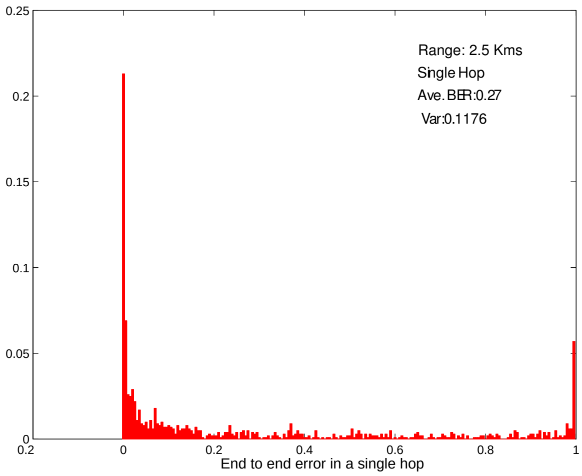

(a)

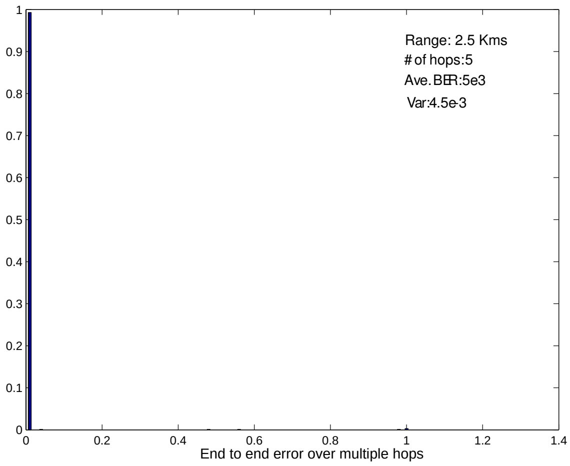

(b)

Figure 5.8: Error distribution for rainy/snowy weather conditions: (a) Single hop FSO link (b) Multi-hop FSO link.

5.5 Multi-Hop system: Amplified Relaying

In amplified relaying, each intermediate terminal simply amplifies the received signal from the immediately preceding terminal. Due to this, the noise also gets amplified by each intermediate terminal and hence is propagated end to end. Any error due to decoding thus is present only at the end receiver and the delay due to relaying by the intermediate terminals is minimized.

At each hop, the received signal plus noise is amplified. Hence, the received SNR is same as the transmitted SNR. Noise gets added to the signal at each hop by N_o. For N hops, the received signal can be expressed as:

$$SNR_{NthHop} = \frac{SNR}{N \cdot N_o}$$

The error behavior for such systems is work in progress; it can be shown that the BER gain and the variance gain in the case of the amplifying system is smaller than that for the decoding system.

5.6 Future Directions

We showed that using multiple hops reduces the mean and variance of the error for the same end-to-end link range. As the number of hops is increased, the error behavior improves, at a cost of increased delay at each hop. Optimizing the tradeoff between errors and end-to-end delay in a multi-hop scenario an interesting problem for future work. Simultaneously optimizing the system reliability, given constraints on the overall system infrastructure costs in multi-hop scenario is another interesting future problem.

The future directions for this work is listed as below:

- Include the effects of turbulence, in addition to geometric and atmospheric attenuation which causes additional distortion of the signal at the receiver in the error model.
- Model burst errors caused by obstructions etc, in addition to the random errors caused by atmospheric effects.
- Remove the Gaussian assumption on the visibility and use an empirical distribution.
- Obtain an expression for outage probability based on a threshold BER.
- Come up with an appropriate FEC scheme that works well for the error characteristics of an FSO channel

CHAPTER 6
Node Localization using Range and Orientation with Free Space Optics

6.1 Introduction

Scalable network localization is key for realizing ad-hoc networks. In this chapter we propose a localization scheme where nodes form a relative coordinate system of the network in a distributed manner. Each node in the ad-hoc network is capable of estimating both the range and orientation of its 1-hop neighbors. The proposed localization scheme then achieves a relative coordinate system for any topology as long as the underlying graph is connected, irrespective of the node density. We evaluate the performance of the proposed scheme and show with simulations that it is more scalable than a similar localization scheme that uses triangulation. We also present propagation of localization error in the network due to estimation errors in both the range and the orientation. We also discuss how this scheme can be implemented using optical wireless technology.

Ad-hoc networks benefit from node localization as it enables stateless geographic routing within the network [32]. In sensor networks, localization makes information from the sensors more meaningful. The most important aspect of the localization algorithm is scalability, specially when applications with thousands of sensor nodes are envisioned for the future. Both ad-hoc and sensor networks ideally require localization be achieved with few or no anchor nodes, with low density deployment of the nodes in the network, and with minimally centralized infrastructure to support localization and mobile node tracking. Node density cannot always be counted on, specially when ad hoc nodes are sprinkled from an aeroplane onto a geographic location, as often described in literature. In addition the localization scheme should accommodate changes in the network topology with very small or no additional control messaging overhead and should be robust to mobility of the nodes in the network.

The problem of end-to-end wireless geographic routing using network local-

L3: Geographic Routing using Node IDs (eg. GPSR)
L2: ID to Location Mapping (eg. DHT, GLS etc.)
L1: Node localization

Figure 6.1: Classification of research issues in distributed localization.

ization can be broadly categorized into three layers as shown in Figure 6.1. The lowest layer addresses the localization scheme to obtain the node coordinates. And the second layer maps these coordinates to the node "Identifiers" like a name or a number [40], [49] . The third layer uses these identifiers to perform stateless geographic routing [32]. A successful network localization scheme addresses all the three layers, localization to routing in a distributed, and scalable manner. In this chapter we focus on the first layer, to localize the nodes and obtain their coordinates in a distributed manner.

Typically in a geographic localization scheme an estimate for "distance" between the nodes is obtained either by the number of hops [42], [48] or an RTT [16], or an explicit range [9] or orientation [43] and then it is translated into virtual or (global or relative) physical coordinates using triangulation. In triangulation, each node needs to communicate with *three* already localized nodes to compute its own location. Therefore, in order to implement a distributed localization scheme using triangulation, a very high node density and a very high average node degree are needed to achieve acceptable node localization percentages (for example, localization for a ring topology is hard to achieve using triangulation). In the past literature, the average node degree ranged from 6 to 16 [38], [43], [9],[54], [51], [52], [11] to achieve a reasonable coverage (extent of node localization).

In this chapter we propose an approach to obtain relative coordinate system in an ad-hoc network scenario where node localization can be achieved with a *single* localized neighbor. The method uses both range and orientation information between the adjacent nodes. The method achieves 100% node localization as long as the underlying graph is *connected*, irrespective of the average node degree and node density. The method does not require any anchor or landmark nodes. Any randomly placed node can become the origin of the relative coordinate system and nodes can obtain their coordinates in a distributed manner with respect to this origin. We evaluate our localization algorithm and show the improvement in performance in terms of the percentage of network localization, number of iterations needed to obtain the relative coordinate system and the number of control messages needed. We also study the error in localization due the range and orientation estimation errors and how it propagates with the number of hops away from the origin in the relative coordinate system.

In methods where triangulation is used, either range or orientation estimates are obtained to come up with the coordinate system for the network. Therefore, nodes are assumed to have the hardware capability to measure either the range or orientation of the neighboring nodes. Though this is a simple requirement from the hardware capability point of view, triangulation itself puts a very high demand on the network topology in terms of node density and average node degree. In addition, to achieve the network coordinate system in a distributed manner, the method may require a few beacon/landmark nodes. On the other hand, our method does not demand high node density or degree from the network but needs that the node be able to measure both the range and orientation of the neighboring nodes. The benefit is that node localization can be achieved with a *single* neighbor.

Our scheme results in a relative coordinate system of the network without any anchor nodes and network wide floods in a distributed manner. An additional benefit of the proposed method is that it can be easily extended for mobile tracking. Due to space limitation we limit the scope of our chapter to static network localization.

The method described in this chapter can be implemented with any physical layer technology, provided that a node capable of measuring both the range and the orientation of its 1-hop neighbors. We propose to implement the present scheme with Optical wireless, which we refer to as Free-Space Optics (FSO) communication technology in the chapter. FSO uses light for communication between two nodes with air as the medium [19]. FSO is known for its high bandwidth, low power per bit and easy deployment. We propose to use the "directionality" of the light beams to measure the orientation between the two nodes and time-of-flight between two nodes to measure the range, thus obtaining the position "vector" of any node relative to

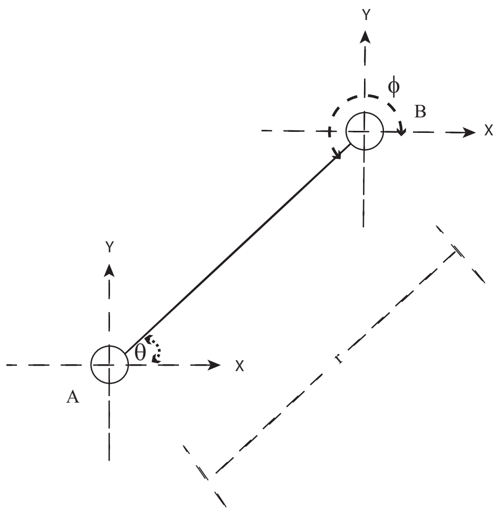

Figure 6.2: Illustration of the principle of an FSO based location system.

another.

The chapter is organized as follows: Section 6.2 we describe the principle of localization, and illustrate with simulations the algorithm for the proposed localization scheme and its evaluation. Section 6.3.1 we discuss how the error is propagated. Section 6.4 We briefly discuss the details on how the nodes can be implemented using FSO technology to have the hardware capabilities to measure the orientation and the range. Section 6.5 describes how we can easily extend our localization method for mobile tracking without any infrastructure. Section 6.7 concludes the chapter with future directions for this work.

6.2 FSO Localization Scheme

6.2.1 Principle

Figure 6.2 illustrates the principle of our localization scheme. Two nodes A and B are such that the perpendicular axes through each of them are aligned with each other. Then, any node, in this case, node A measures the range r and the orientation θ of its 1-hop neighbor, node B and computes the coordinates of the node B, with itself at the origin as following:

$$x_b = rcos\theta$$

$$y_b = rsin\theta$$

If node A is already localized with coordinates (x_a, y_a) then the coordinates of node B can be obtained by simple vector addition:

$$x_b = x_a + rcos\theta$$

$$y_b = y_a + rsin\theta$$

Thus each node can compute its 1-hop neighbors coordinates relative to itself. A leader is selected to be at the origin and a relative coordinate system of the entire network can be obtained in a distributed manner. Thus this scheme requires only *one* already localized node for any given node to localize. When the underlying graph is connected, we can have all the nodes in the network (100% coverage or extent) localized.

In contrast, triangulation needs at least three localized nodes to obtain node localization. Typically these nodes are the landmark nodes and their location in the network plays a significant role on the extent of localization. And the anchors need to know that they are indeed the anchor nodes. Moreover, triangulation needs a high average node degree and high node density to achieve a reasonable percentage (coverage) of node localization.

The attractive part of the technique is that the final coordinate system can be achieved even when the network is sparse, as long as the graph is connected. Our scheme needs additional hardware capability for a node to measure both the range and orientation of the neighboring nodes. At the end of the algorithm, we obtain a relative coordinate system with an elected leader at the origin. Once the initial relative coordinate system is obtained, the origin is independent of the position of the leader node. And all the nodes are free to move, and the location of the origin is preserved. Our approach does not need any network wide flooding or anchor nodes for synchronization and does not depend on the knowledge of the network topology.

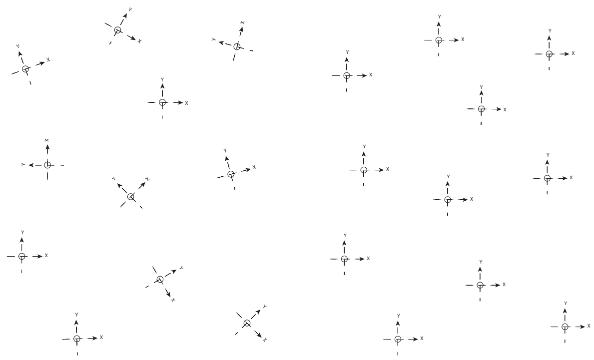

(a) (b)

Figure 6.3: (a) Nodes before localization. (b) Nodes after localization.

6.2.2 Assumptions and Problem Definition

We assume that each node has a set of perpendicular axes passing through it as shown in Figure 6.2. We assume that the FSO nodes have the capability to measure the range of the 1-hop neighbors and the orientation of the neighbor. In addition, each node is also capable of re-orienting the axes passing through it. We will explain how these capabilities can be achieved using nodes with Free-space Optical transceivers. Further, the nodes in the network have unique IDs, which are used to elect a leader. We assume that network is connected and all the nodes at bootstrap have $(0, 0)$ as coordinates.

Then, the network localization problem is defined as follows: At bootstrap, the nodes are randomly located. At bootstrap, the axes of different nodes are oriented randomly with respect to each other. All the nodes in the network graph are as shown in Figure 6.3.a . The objective of the FSO localization algorithm (FLA) is to orient the axes of all the nodes such that they are parallel to each other as shown in Figure 6.3.b. This is achieved between any two nodes by measuring the orientations of each other and exchanging that information. This procedure is explained in Section 6.2.4. After that step, each node then estimates the "direction" at which the neighbor is located by measuring the angle with respect to its X-axis. Then, the nodes jointly obtain a relative coordinate system in a distributed manner.

6.2.3 FSO Localization Algorithm

The FSO localization algorithm has three phases. First, the node with the "highest ID" is elected as the leader in a distributed manner. Then all the nodes align their axes with the leader node's axes. Then each node computes the coordinates of its neighbors with lower IDs.

At bootstrap each node communicates with all its 1-hop neighbors and the IDs of the neighbors are exchanged. Each node becomes aware of the 1-hop neighbor with the highest ID and axes orientation and saves that information. Whenever a node updates to a new higher neighbor ID, it broadcasts the same to its 1-hop neighbors. This process of exchanging the highest ID happens until there are no updates at any node. At that time, all the nodes in the network are aware of the leader node's ID and its axes orientation information. Each node waits for a pre-assigned time duration and when it does not hear any more broadcasts from its neighbors, it aligns its axes according to the leader node's orientation information. The actual alignment procedure is explained under Section 6.2.4. This completes the leader selection and alignment phase.

Once aligned, each node can measure the range and orientation of its neighbor with a lower ID. When a node computes the coordinates of the nodes with lower IDs it sets the nodes "Highest-CoOrd-ID" to the leader ID. A node becomes eligible to compute the coordinates of the neighboring nodes when it receives its coordinates from a node whose Highest-CoOrd-ID is equal to the leader ID. By default, the leader with the highest ID has this condition satisfied, so it starts to compute the coordinates of its 1-hop neighbors by measuring their range and orientation. The leader thus establishes itself as the origin. The 1-hop neighbors of the leader node receives their coordinates from the leader and update their coordinates. These 1-hop neighbors of the leader, in turn become eligible to calculate the coordinates of their 1-hop neighbors who have not already received the coordinates from the leader. The relative coordinates with respect to the leader, are calculated using the vector addition described in Section 6.2.1. The pseudo-code of the algorithm is shown in Algorithm 1.

After the localization is complete, the location of the leader node can then be

Algorithm 1 Localization

if $MyLeaderIDChangeFlag = 1$ **then**
  UPDATE and broadcast to neighbors of this new highest ID
end if
repeat
  Listen for more updates from the neighbors
  if Received a broadcast from the neighbor **then**
    if $ReceivedID > MyLeaderID$ **then**
      $MyLeaderID = ReceivedID$ and $MyLeaderIDChangeFlag = 1$
    else if $MyLeaderIDChangeFlag = 0$ **then**
    end if
  end if
until No broadcast from the neighbors for time T
ALIGN axes with the highestID neighbor
if $HighestCoOrdID = LeaderID$ **then**
  COMPUTE coordinates of neighbors with lower ID
end if

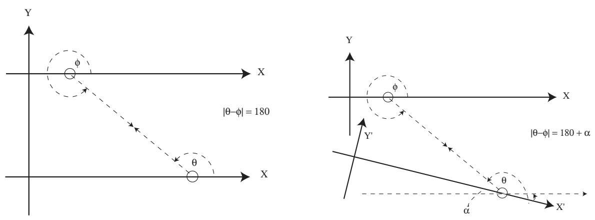

(a) (b)

Figure 6.4: (a) Aligned nodes with parallel axes. (b) Non-aligned nodes.

considered as "Virtual Origin Node" O. Since at the time of initial localization, the positions of each of the nodes are determined by this location, the localization does not get affected even if the leader node is changed or moved. This feature makes this localization scheme robust to node movements. If a new node joins the network it simply communicates with the nearest neighbor and calculates its coordinates from its position with respect to the neighbor and the neighbor's coordinates with respect to O, irrespective of its ID. A node that either goes into sleep or dies will not have any affect on the coordinate system.

6.2.4 Alignment

The alignment procedure for the nodes needed in our localization scheme is explained here. Consider two FSO nodes as shown in Figure 6.2. A sees B at (θ, r)

and B sees A at (ϕ, r). The two nodes exchange this information while aligning. When the axes of A and B are aligned, as shown in Figure 6.4(a), $|\theta - \phi| = 180$. When the axes are not aligned, say by an angle $\pm\alpha$, then the equation becomes $|\theta - \phi| = 180 \pm \alpha$. The method is illustrated in Figure 6.4(b). Depending on who the leader is, for example if node A has a higher ID than node B, node B aligns itself with node A. When the nodes are aligned with each other, then the node with the higher ID becomes the reference and the node with the lower ID simply accepts the coordinates given by the node of the higher ID.

6.3 Performance of the Localization Algorithm

We evaluated the performance of our localization algorithm for scalability using the following metrics,

- Extent of node localization
- Convergence time
- Number of messages per node to localize in the relative coordinate system.

We will discuss each of them below. We simulated for random networks in a area of 200×200 Sq. units for two node densities, 100 nodes and 400 nodes. We compared the metrics against a simple distributed triangulation scheme with three landmark nodes. Bear in mind that the triangulation scheme *does not* give a relative coordinate system, but just localizes the nodes relative to three landmark nodes. Whereas with our scheme, we obtain a coordinate system, with an origin and the coordinates of the nodes with respect to the origin. We observe that even the simple version of triangulation performs worse than our scheme.

As mentioned in the previous section, with our scheme, all the nodes in the network are localized if the underlying graph is connected. Thus, the extent of localization is always 100%, irrespective of the average node degree of the graph. Figure 6.5 illustrates the 100% localization achieved using this algorithm. The figure also illustrates how triangulation needs a high average node degree to achieve a reasonable extent of localization.

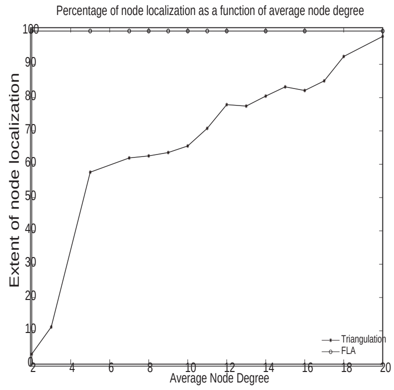

Figure 6.5: Extent of localization as a function of average node degree.

The second metric is the convergence time on the algorithm, which we measured as the number of iterations needed to achieve 100% localization. Each iteration is defined as a new update of the highest ID at a node and the broadcast associated with it. We count the maximum number of iterations needed for all the nodes to localize. Since leader election and identification is implemented in a hop-by-hop manner, the maximum number of iterations taken by the algorithm is a function of how many hops away a node is from the leader node being selected. In Figure 6.6 the number of iterations taken by the algorithm to achieve 100% localization is shown as a function of the average node degree. As the node degree increases, the number of iterations needed to localize decreases, since the information about the leader node spreads more quickly. Whereas as the node density in the network increases, the number of iterations increase because then hop length becomes smaller and the number of hops from the leader node increases.

Figure 6.7 compares the number of iterations taken by triangulation and our scheme. Our scheme out performs triangulation for all node degrees.

Figure 6.8 shows the average number of messages each node needs to localize. The number of messages for higher node density is higher because of higher number of iterations needed. As we observed, the number of messages increase linearly with node degree. Figure 6.9 shows that the number of messages needed for localization is independent of the node density, making the algorithm more scalable.

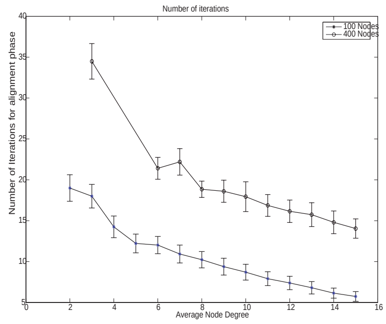

Figure 6.6: Number of iterations needed to localize as a function of average node degree.

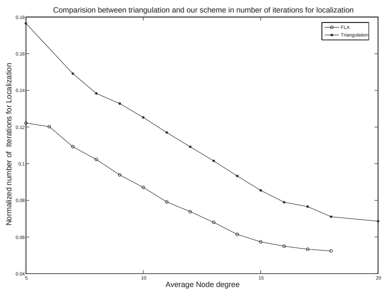

Figure 6.7: Comparison of the number of iterations for localization for FLA and triangulation.

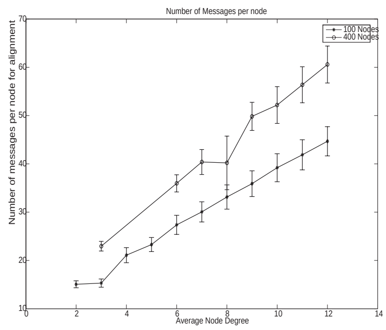

Figure 6.8: Number of messages per node for alignment and leader selection as a function of average node degree.

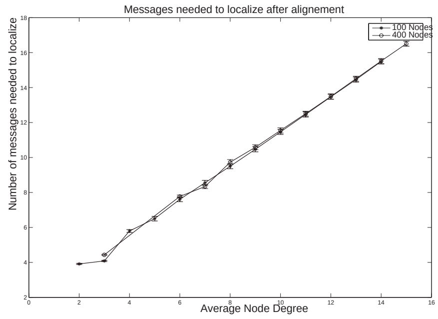

Figure 6.9: Number of messages per node for localization as a function of average node degree.

6.3.1 Measurement Errors and Accuracy of Localization

In this section we evaluated the robustness of our localization scheme in the presence of measurement errors in both the range and the angle. The error creeps into the location system from the following sources:

- Finite field of view of the photo-detectors: This effects the alignment angle.
- Finite package density of the transceivers. This too effects the alignment angle.
- Measurement error of the range r.

As shown in Figure 6.12, the transceiver a has a finite field of view, a magnitude denoted by the angle ϕ. Consequently, the transceiver, when trying to measure the orientation at which it "sees" another node, the angle becomes $\theta \pm \phi/2$. A similar error results when the number of transceivers on the FSO node are few, thereby reducing the resolution of the angle with which a neighbor is perceived. In our simulation we introduced an error of $\pm 20\%$ in the measurement of both range and orientation. Figure 6.11 shows how percent error in X, Y co-ordinates due to measurement errors in range behave with the number of hops from the leader node. The simulations show the worst case error results. The error stays constant at 20% for all the hops. Figure 6.10 shows how the "absolute" error due to an estimation error in both the angle and range propagates with the number of hops from the origin (leader node). The plot shows an linear increase due to the range error as expected. The error due to an error in angle is much more pronounced than that

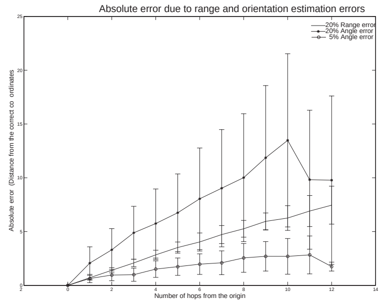

Figure 6.10: Absolute error in terms of distance from correct coordinates.

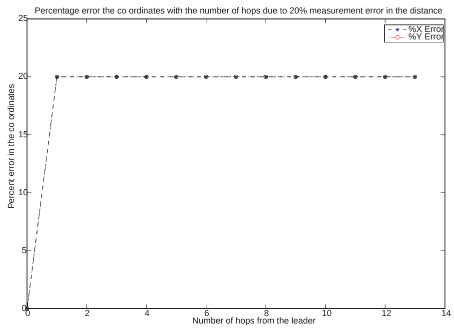

Figure 6.11: Percent error in X, Y coordinates as a result of measurement error in range.

of the range. Figure 6.10 also shows an improvement in the error behavior when the number of transceivers on the FSO node is increased. For the lower error, we are increasing the number of transceivers on the FSO node and also decreasing each transceivers field of view. This will decrease the value of ϕ as shown in Figure 6.12.

6.4 FSO System

In this section we discuss how to realize a practical scheme to implement the measurement of both the angle and the range between two communicating nodes. Typically in RF technology, range is measured using TDOA or signal strength of the received signal [47], [53], [5], [42]. There are currently techniques available in RF to obtain orientation [43] and the range information of a neighbor. In this section we will describe how a practical system can be implemented using free-space-optical technology. Since the primary focus of the chapter is to introduce our localization scheme, but not the hardware implementation, we describe the

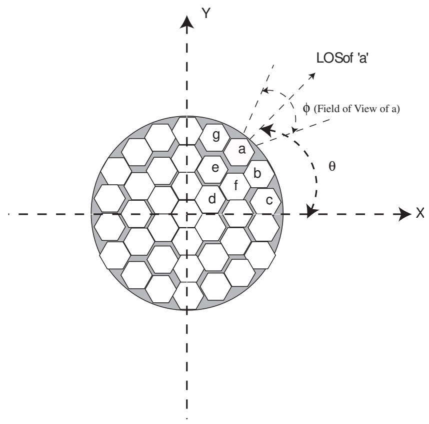

Figure 6.12: FSO antenna for localization.

implementation briefly. More details on this implementation are in [3].

We propose to use the “directionality” of the optical signals to measure the orientation of the neighbors. In our implementation, each node is equipped with multiple optical transceivers as shown in Figure 6.12. Each transceiver on the node has a direction defined by its line of sight, in this scheme it coincides with the X-axis of the node. Each transceiver also has a finite field of view denoted by ϕ, the X-axis being right in the middle of the field of view. And the orientation of the neighbor is measured with respect to this axis. Since FSO communication is directional, there is no interference as experienced in RF.

Each transceiver can both receive and send signals to and from its 1-hop neighbors it is directly in view with. These systems can be implemented using off-the-shelf components. The density with which the transceivers are tessellated on the node and the field of view of these transceivers decides the accuracy that can be obtained while measuring the orientation of the 1-hop neighbor. On the other hand, the range error depends on the electronics used to compute the time-of-flight information between two nodes. The time-of-flight can be stretched artificially so as to be able to measure using off-the-shelf electronics.

Each node has a set of perpendicular axes going through it. By identifying the location of individual transceivers, a node can recognize the orientation of the axes with respect to itself. To re-orient the axes, the node just needs to shift its reference. Thus each node equipped with optical transceivers and a processing capability can be used for network localization using our scheme.

6.5 Mobile tracking

Our localization scheme can be extended easily to handle mobility of the nodes. The combination of having the initial coordinate system with respect to a virtual (not attached to any physical node) origin and having the axes of all the nodes aligned can be very effectively used to obtain a distributed GPS-like environment, where mobile nodes can self compute their coordinates as they move. In literature mobile tracking techniques depended on a central infrastructure to achieve node mobility [46] [56], whereas our approach does not need any. A node equipped with a capability of measuring the angle and distance (basically, velocity) by which it moves, can easily self compute the new coordinates after a displacement by just performing a simple vector addition. These capabilities as similar to inertial navigational systems, which can be implemented on MEMS to achieve the form factors suitable for ad-hoc and sensor networks [64]. Figure 6.13 illustrates the concept. As shown the coordinates of the nodes A and B after they are moved are shown are with respect to the origin O, which is fixed and can be made to be external to any node, as soon as the initial localization of the static network is achieved.

6.5.1 Concept of Virtual Origin

Each node in our localization scheme has a set of references axes, parallel to the axes at the origin of the relative coordinate system. The coordinates of the nodes after initial localization reflects the relative position of the origin from the node, its position vector. Even if the actual physical node at the origin moves, the position vector of any other node does not change, thereby preserving the relative *virtual* origin position. This is the interesting feature of our localization scheme. With this feature, supposing that a node has the ability to monitor its velocity, both the direction of the movement and the speed, like an inertial navigation system, a node can self compute its coordinates after displacement. Thus any node in the network is aware of the *virtual* origin position. For a node to self compute its coordinates after displacement, the node should be capable of the following two things:

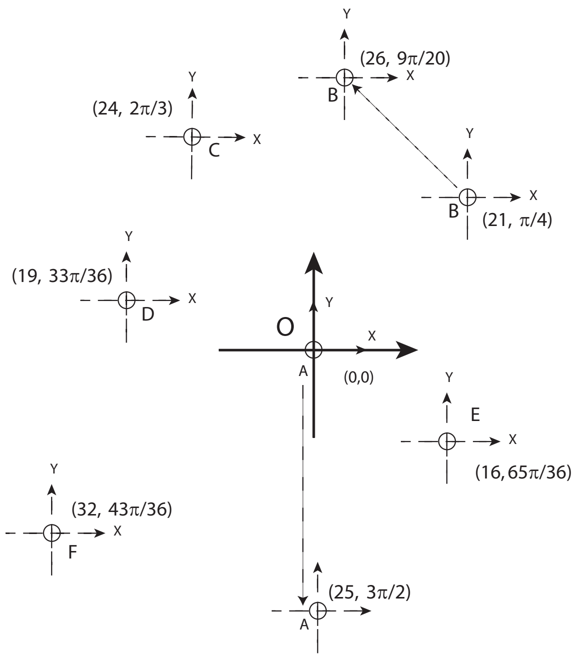

Figure 6.13: When the node can measure its velocity and preserve the axes orientation

- Preserve the orientation of its reference axes parallel to the ones at the origin.
- Measure the direction and the speed with which it is moving, and the duration.

To preserve the orientation while moving in any random direction, a node should be equipped with a compass. And to measure the velocity, a gyroscope, or an inertial navigation system is needed. According to the new developments in the navigation technology, it is possible to embed MEMS based navigation systems in an ad hoc node satisfying the form factors. If the node has the above to abilities, it can self compute its coordinates after motion (better yet, while moving).

In the following section, we examine several scenarios with varying node capabilities and assumptions so as to be able to self-compute its coordinates.

6.6 Computation of coordinates after movement

In this section we discuss several possibilities for nodes to self compute their coordinates after they move to a new location. Nodes can simply have the knowledge of their displacement vectors and self compute the coordinates without the need of external help. Otherwise, two nodes after they move into a new location can become neighbors and collaborate to find their new coordinates in a distributed manner. These scenarios are outlined below:

1. **Scenario I.**

   Assumptions:

   - Node can measure its velocity, i.e, both the speed and direction of movement.
   - Node preserves the orientation of the axes.

   These assumptions are similar to having an INS (inertial navigation system) or node being equipped with a compass and an accelerometer. The node then knows its displacement *vector*, therefore can self compute its new co-ordinates by performing simple vector addition.

2. **Scenario II.**

   Assumptions:

   - When a mobile node has a already localized node in its new neighborhood

   This assumption is same as having a localized stationary neighbor in the mobile node's new vicinity. In this case, the mobile node simply aligns itself with the new node and estimates its range and orientation from the localized neighbor and simply computes its coordinates by preforming vector addition. How the localized neighbor is already localized is another question. It might be inherently assumed that some nodes are equipped with INS and other just contact these more capable nodes to localize after movement.

3. **Scenario III.**

   Assumptions:

   - Node preserves the orientation of the axes.

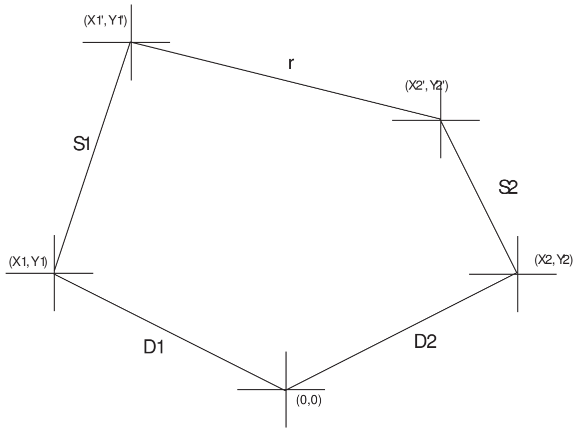

Figure 6.14: Two nodes moving while preserving their axes orientation, know speed but not velocity

- Nodes can measure the distance moved, but cannot measure which direction they are moving.

This assumption means that the nodes are equipped with a compass, but not a navigation system. The direction of the node movement is not known but the axes orientation is preserved to be parallel with the reference axes at the virtual origin. The speed of the mobile node is known, but not the velocity.

We assume that the mobile node has at least one neighbor in its new location. If the neighbor is already localized, then it is just Case2. In this section we consider the situation if the new neighbor is not already localized. In this case, the two nodes cooperate and exchange information so as to compute their coordinates. We can show that this method does not yield a unique solution, so the nodes new coordinates cannot be found out.

As seen from Figure 6.14, the four nodes form a quadrilateral for which the lengths of the sides are known. Since the axes orientation is preserved, the angle with which the side joining the two new node positions with the X-axis is also known.

We tried two solution approaches, one using the projections of the sides of the quadrilateral on the X-axis and Y-axis respectively, shown in Figure 6.15. We get two trigonometric equations with the two unknowns, namely, θ, and Ψ.

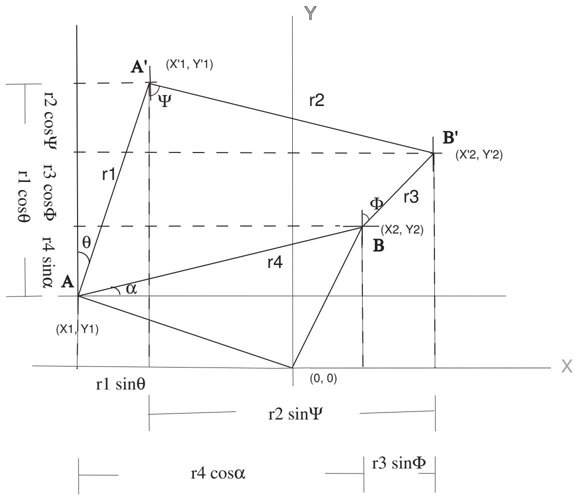

Solution based on Length Projections

Figure 6.15: Solution approach based on the projection of the sides

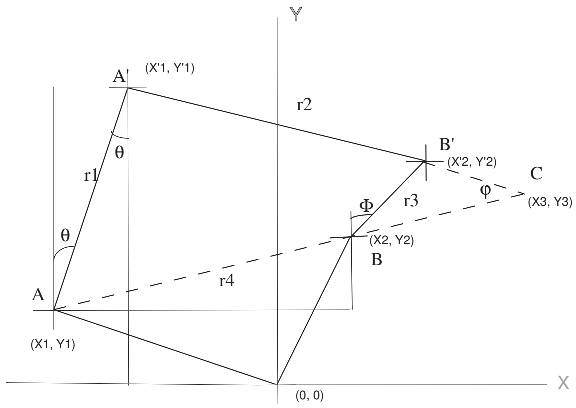

Solution based on the ratios of the sides of a triangle

Figure 6.16: Solution approach based on the projection of the quadrilateral to a point

$$r_4cos(\alpha) + r_3sin(\Phi) = r_1sin(\theta) + r_2sin(\Psi)$$

$$r_1cos(\theta) = r_2cos(\Psi) + r_3cos(\Phi) + r_4sin(\alpha)$$

The second solution approach is by taking the ratios of the triangles formed by projecting the quadrilateral as shown in Figure 6.16.

Consider the triangles $AA'C$ and $BB'C$ in Figure 6.16. Following the Law of sines:

$$\frac{sin(\Psi)}{r_1} = \frac{sin(A')}{r_4 + r_5}$$
$$\frac{sin(\Psi)}{r_3} = \frac{sin(B')}{r_5}$$

We can infer the values of θ and Φ from A' and B' respectively. The angle Ψ is obtained by finding the angle between the two straight lines $A'B'$ and AB as following:.

Equation of the straightline AB is given by:

$$\frac{y - y_1}{x - x_1} = \frac{y_2 - y_1}{x_2 - x_1}$$

But there is no way we can determine the equation of the straight line $A'B'$. With this approach, the system is underdetermined, so cannot be solved to find a unique solution.

4. **Scenario IV.**

   Assumptions:

   - Node moves such that the node head, represented by its Y axis moves in the same direction as the node.
   - The speed of the mobile node is known, but not the velocity.

   This mode of mobility will yield a unique solution if the nodes axes are aligned before movement.

   Proof of Uniqueness for Scenario IV

   In this case, as seen in Figure 6.17, the lengths of all four sides of the quadrilateral $AA'BB'$ are specified. AA' and BB' from the speed of the node, $A'B'$ by measuring and AB by the knowledge of the previous coordinates of the both nodes after information exchange. In addition, the angles $AA'B'$ and $BB'A'$ can be obtained by measuring the orientation of A' and B' with respect to each

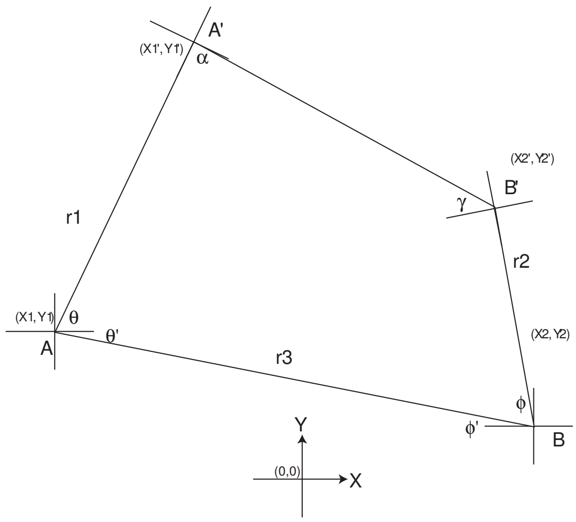

Figure 6.17: Two nodes moving such that the head is pointed in the direction of motion, know their individual speed but not velocity

other. This *fully* specifies the quadrilateral. So the quadrilateral is unique. (It would be nice to have a more formal proof)

So in this system, the nodes after moving will form a uniquely specifiable quadrilateral. Now, we outline a method by which it is achieved and the new coordinates of nodes are obtained.

The assumption are that the axes of the nodes are aligned to the X- and Y-axes of the network coordinate system and therefore with each other. This can be accomplished by a periodical refreshing or alignment of the axes orientation through the entire network.

Applying the Law of Cosines two times, we can arrive at the coordinates of the two mobile nodes. The lengths of the diagonals d_1 and d_2 can be found as:

$$d_1^2 = r_1^2 + r_4^2 - 2r_1r_4cos(\alpha)$$

$$d_2^2 = r_4^2 + r_2^2 - 2r_4r_2cos(\gamma)$$

Using the values of d_1 and d_2, we find the unknown angles θ and ϕ.

$$d_1^2 = r_3^2 + r_2^2 - 2r_3r_2cos(\theta + \theta^1)$$

$$d_2^2 = r_1^2 + r_3^2 - 2r_1r_3cos(\phi)$$

Using θ and ϕ and r_4, the new coordinates are computed as:

$$X_1^1 = X_1 \pm rcos(\theta)$$

$$Y_1^1 = Y_1 \pm rsin(\theta)$$

$$X_2^1 = X_2 \pm rcos(\phi)$$

$$Y_2^1 = Y_2 \pm rsin(\phi)$$

The problem now is to figure out the $\pm$. (Into which quadrant did the node move relative to itself)? This can be found out from the relative angles in a specific quadrilateral.

6.7 Future Directions

The future directions for the localization problem are:

- Evaluate the performance of our mobile tracking algorithm in terms of its scalability and robustness to error propagation.
- Proof of uniqueness of the quadrilateral to prove that the coordinates we get in mobile tracking are unique, i.e., there is no ambiguity.
- Implementation of a distributed name-to-address mapping for mobile ad hoc network

CHAPTER 7
Future Directions

In this chapter, we briefly describe the issues we are going to address to complete and improve the results we have obtained so far and add new contributions.

7.1 2-Dimensional FSO antennas

We demonstrated bandwidth gains in short rage FSO communication using 2 dimensional FSO antennas. We would like to extend the applications of such arrays to provide reliability to over come temporary obstructions and other atmospheric effects by implementing suitable error codes that exploit the spatial re-use/redundancy. The specific issues to be addressed to achieve this are:

- Include the Gaussian noise in the interference model, to remove the ambiguity in obtaining the expression for inter-channel interference.

  In the noise computation, only the inter-channel interference is considered, as Gaussian noise effects equally all the channels. Inclusion of Gaussian noise makes the model more complete, but may not add any additional insight on the array performance in terms of its parameters.

- Coming up with an FEC scheme that exploits the "space" on the array:

  The multiple channels in the array can be used to add redundancy to the communication link to improve its reliability. Unlike MIMO, channels on the FSO array are highly correlated as they are spatially close to each other. Because of this, there is no "diversity gain". The possible design choices are to stagger the data streams in time and space, or provide link protection just by sending duplicate data steams etc.

7.2 Multi-hop FSO Communication

In modeling the end-to-end random errors, we considered geometric and atmospheric attenuations. We would like to improve the error modeling by considering the burst errors are well. The model can be made more complete by including the effects of atmospheric turbulence. Obtaining an expression for outage probability of an FSO communication link will provide more insights into the system design.

7.3 Localization and Mobile tracking using FSO

We would like to implement our localization scheme and name-to-address mapping on the spherical antennas. By using existing routing protocols like GPSR, we will evaluate perforce of our localization frame work in stationary and mobile situations. Towards achieving this, the more specific issues to be addressed are:

- Include the literature on mobile tracking and mobility models.
- Evaluate the performance of our mobile tracking algorithm in terms of its scalability and robustness to error propagation.
- Proof of uniqueness of the quadrilateral to prove that the coordinates we get in mobile tracking are unique, i.e., there is no ambiguity.
- Implementation of a distributed name-to-address mapping for mobile ad hoc network

BIBLIOGRAPHY

[1] A. Acampora and S. Krishnamurthy. A broadband wireless access network based on mesh-connected free-space optical links. In *IEEE Personal Communications*, pages 62–65, October 1999.

[2] http://www.semiconductor.agilent.com.

[3] J. Akella, C. Liu, D. Partyka, M. Yuksel, S. Kalyanaraman, and P. Dutta. Building blocks for mobile free-space-optical networks. In *Proceedings of IFIP/IEEE International Conference on Wireless and Optical Communications Networks (WOCN)*, pages 164–168, Dubai, United Arab Emirates, March 2005.

[4] Baha.E.A., Saleh, and M. Teich. *Fundamentals of Photonics.* Wiley-Interscience, 1991.

[5] P. Bahl and V. N. Padmanabhan. Radar: An in-building rf-based user location and tracking system. In *IEEE INFOCOM*, Israel, 2000.

[6] S. Bloom, E. Korevaar, J. Schuster, and H. Willebrand. Understanding the performance of free-space optics. *Journal of Optical Networks*, 2(6):178–200, June 2003.

[7] M. Blume, F. McCormick, P. Marchand, , and S. Esener. Array interconnect systems based on lenslets and cgh. In *Technical Report 2537-22, SPIE International Symposium on Optical Science Engineering and Instrumentation*, San Diego, 1995.

[8] D. Britz. A review of the concept of availability as it relates to free space optical communications. http://www.wcai.com/.

[9] S. Capkun, M. Hamdi, and J. Hubaux. Gps-free positioning in mobile ad-hoc networks. In *Proceedings of the 34th Annual System Sciences, 2001*, Hawaii, Jan. 2001.

[10] V. Chan. Optical space communications: a key building block for wide area space networks. *IEEE Lasers and Electro-Optics Society*, 1:41–42, 1999.

[11] K. Chintalapudi, R. Govindan, G. Sukhatme, and A. Dhariwal. Ad-hoc localization using ranging and sectoring. In *INFOCOM*, Hong Kong, China, March 2004.

[12] C. Chuah, G. J. Foschini, R. A. Valenzuela, D. Chizhik, J. Ling, and J. Kahn. Capacity growth of multi-element arrays in indoor and outdoor wireless channels. In *Proc. of IEEE Wireless Commun. and Networking Conf.*, Chicago, IL, Sept. 2000.

[13] C. Chuah, D. Tse, and J. M. Kahn. Capacity of multi-antenna array systems in indoor wireless environment. In *Proc. of IEEE Global Commun. Conf.*, Sydney, Australia, Nov. 1998.

[14] C. Chuah, D. Tse, J. M. Kahn, and R. A. Valenzuela. Capacity scaling in dual-antenna-array wireless systems. *IEEE Trans. on Information Theory*, 48:637–650, Mar. 2002.

[15] L. W. Couch. *Digital and Analog Communication Systems*. Printice Hall, 2000.

[16] F. Dabek, R. Cox, F. Kaashoek, and R. Morris. Vivaldi: a decentralized network coordinate system. In *SIGCOMM'04*, Portland, Oregon, USA, Aug. 2004.

[17] T. ElBatt and H.Izadpanah. Design aspects of hybrid rf/free space optical wireless networks. In *2001 IEEE Broadband Communications for the Internet Era Symposium digest*, pages 157 – 161, September 2001.

[18] R. Flickenger. *Building Wireless Community Networks*. O'Reilly and Associates, 2001. 1st Edition.

[19] http://www.freespaceoptics.org/freespaceoptics/default.cfm/.

[20] R. M. Gagliardi and S. Karp. *Optical Communications*. John Wiley and Sons, New York, 1976.

[21] M. S. Gast. *802.11 Wireless Networks: The Definitive Guide*. O'Reilly and Associates, 2002. 1st Edition.

[22] M. Grossglauser and D. Tse. Mobility increases the capacity of ad-hoc wireless networks. In *IEEE Infocom 2001*, April 2001.

[23] P. Gupta and P. R. Kumar. The capacity of wireless networks. *IEEE Transactions on Information Theory*, IT-46(2):388–404, March 2000.

[24] D. Heatley. Optical wireless: The story so far. *IEEE Communications*, 36:72–82, December 1998.

[25] J. Hightower and G. Borriello. Location systems for ubiquitous computing. *IEEE Computer*, 34(8):57–66, Aug. 2001.

[26] W. Hirt, M. Hassner, and N. Heise. Irda-vfir (16 mb/s): Modulation code and system design. *IEEE Personal Communications*, pages 58–71, February 2001.

[27] IEEE. *IEEE 802.16-2001, IEEE Local and Metropolitan Area Networks–Part 16 –Standard Air Interface for Fixed Broadband Wireless Access Systems*, 2001.

[28] IETF. *Mobile Ad-hoc Networks (MANET) Working Group.* http://www.ietf.org/html.charters/manet-charter.html.

[29] International Electrotechnical Commission. *CEI/IEC825-1: Safety of Laser Products*, 1993.

[30] J.Li, C.Blake, D. Couto, H.I.Lee, and R. Morris. Capacity of ad hoc wireless networks. In *ACM International Conference on Mobile Computing and Networking (MobiCom '01)*, Italy, July 2001.

[31] J. Kahn and J. Barry. Wireless infrared communications. *Proc. of the IEEE*, 85:265–298, February 1997.

[32] B. Karp and H. Kung. Greedy perimeter stateless routing for wireless networks. In *Proceedings of the Sixth Annual ACM/IEEE International Conference on Mobile Computing and Networking (MobiCom 2000)*, pages 243 – 254, Boston, MA, August 2000.

[33] G. Kim, X. Han, and R. T. Chen. Crosstalk and interconnection distance considerations for board-to-board optical interconnects using 2-d vcsel and microlens array. volume 12, June 2000.

[34] I. Kim, R. Stieger, C. Moursund, J. A. Koontz, M. Barclay, P. Adhikari, J. Schuster, and E. Korevaar. Wireless optical transmission of fast ethernet, fddi, atm, and escon protocol data using the terralink laser communication system. *SPIE Opt. Eng.*, 37(12):3143–3155, December 1998.

[35] I. I. Kim, B.McArthur, and E. Korevaar. Comparison of laser beam propagation at 785 nm and 1550 nm in fog and haze for optical wireless communications. In *http://www.opticalaccess.com/news-white-papers.shtml*.

[36] A. M. Ladd, K. E. Bekris, A. Rudys, L. E. Kavraki, D. S. Wallach, and G. Marceau. Robotics-based location sensing using wireless ethernet. In *MOBICOM'02*, Atlanta, Goergia, USA, September 2002.

[37] S. G. Lambert and W. L. Casey. *Laser Communications in Space.* Artech House, Boston, MA, 1995.

[38] K. Langendoen and N. Reijers. Distributed localization in wireless sensor networks: a quantitative comparision. *Elsevier Computer Networks*, 43(2003):499–518, 2003.

[39] J. Li, C. Blake, D. D. Couto, H. Lee, and R. Morris. Capacity of ad hoc wireless networks. In *Proceedings of the 7th ACM International Conference on Mobile Computing and Networking (MobiCom)*, 2001.

[40] J. Li, J. Jannotti, D. S. J. D. Couto, D. R. Karger, and R. Morris. A scalable location service for geographic ad hoc routing. In *ACM MOBICOM*, pages 120–130, Boston, MA, 2000.

[41] http://www.lightpointe.com/.

[42] D. Niculescu and B. Nath. Ad hoc positioning system (aps). In *GLOBECOM 2001*, San Antonio, Nov. 2001.

[43] D. Niculescu and B. Nath. Ad hoc positioning system (aps) using aoa. In *INFOCOM 2003*, pages 1734–1743, Mar. 2003.

[44] http://www.opticalaccess.com/news-white-papers.shtml.

[45] G. Pang. Optical wireless based on high brightness visible leds. In *IEEE Industry Applications Conference*, pages 1693–1699, 1999.

[46] N. B. Priyantha, H. Balakrishnan, E. Demaine, and S. Teller. Mobile-Assisted Localization in Wireless Sensor Networks. In *IEEE INFOCOM*, Miami, FL, March 2005.

[47] N. B. Priyantha, A. Chakraborty, and H. Balakrishnan. The cricket location-support system. In *Proc. of the Sixth Annual ACM International Conference on Mobile Computing and Networking (MOBICOM)*, aug 2000.

[48] A. Rao, S. Ratnasamy, C. Papadimitriou, S. Shenker, and I. Stoica. Geographic routing without location information. In *MOBICOM'03*, San Diego, CA, Sept. 2003.

[49] S. Ratnasamy, B. Karp, S. Shenker, D. Estrin, R. Govindan, L. Yin, and F. Yu. Data-centric storage in sensornets with ght, a geographic hash table. *MONET*, 8(4):427–442, 2003.

[50] T. Sakano, K. Noguchi, and T. Matsumoto. Novel free-space optical interconnection architecture employing array devices. *Electronics Letters*, 27(6):515–516, Mar. 1991.

[51] C. Savarese, K. Langendoen, and J. Rabaey. Robust positioning algorithms for distributed ad-hoc wireless sensor networks. In *USENIX Technical Annual Conference*, pages 317–328, Monterey, CA, 2002.

[52] C. Savarese, J. Rabaey, and J. Beutel. Location in distributed ad-hoc wireless sensor networks. In *Proceedings of Acoustics, Speech, and Signal Processing, 2001.*, pages 2037–2040, May 2001.

[53] A. Savvides, C.-C. Han, and M. Srivastava. Dynamic fine-grained localization in ad-hoc networks of sensors. In *ACM MOBICOM*, Rome, Italy, 2001.

[54] A. Savvides, H. Park, and M. Srivastava. The bits and flops of the n-hop multilateration primitive for node localization problems. In *First ACM International Workshop on Wireless Sensor Networks and Applications*, pages 112–121, Atlanta, GA, 2002.

[55] F. Shubert.

[56] A. Smith, H. Balakrishnan, M. Goraczko, and N. B. Priyantha. Tracking Moving Devices with the Cricket Location System. In *2nd International Conference on Mobile Systems, Applications and Services (Mobisys 2004)*, Boston, MA, June 2004.

[57] M. Steege. *Free-Space Optics: A Viable, Secure Last-Mile Solution?* Sans Institute, 2002.

[58] S. Tang, R. Chen, L. Garrett, D. Gerold, and M. M. Li. Design limitations of highly parallel free-space optical interconnects based on arrays of vertical cavity surface-emitting laser diodes, microlenses, and photodetectors. *Journal of Lightwave Technology*, 12(11):1971–1975, Nov. 1994.

[59] A. Tavares. Experimental characterization of rate-adaptive transmission and angle diversity reception techniques. *IEEE Wireless Communications*, 10(2):–, April 2003.

[60] http://www.terabeam.com.

[61] F. Tooley, R. Morrison, and S. Walker. Design issues in free-space digital optics. In *Third International Conference on Holographic Systems, Compon ents and Applications, 1991*, 16-18 Sep 1991.

[62] D. Tsang, H. Roussell, J. Woodhouse, J. Donnelly, C. Wang, D. Spears, R. Bailey, D. Mull, K. Pedrotti, and C. Seabury. High-speed high-density parallel free-space optical interconnections. In *LEOS '94 Conference Proceedings*, pages 217–218, Oct–Nov 1994.

[63] http://www.uniroyalopto.com/whitepapers/ba1.html.

[64] K. J. Walchko, M. C. Nechyba, E. Schwartz, and A. Arroyo. Embedded low cost inertial navigation system. In *Florida Conference on Recent Advances in Robotics*, Dania Beach, FL, May 2003.

[65] H. Willebrand and B. S. Ghuman. *Free Space Optics*. Sams Pubs, 2001. 1st Edition.

[66] P. W. Wolniansky, G. J. Foschini, G. D. Golden, and R. A. Valenzuela. V-blast: An architecture for realizing very high data rates over the rich-scattering wireless channel. In *Proceedings of ISSSE*, Pisa, Italy, September 1998.

[67] J. Zhang. Proposal of free space optical mesh network architecture for broadband access. In *IEEE International Conference on Communications*, pages 2142 – 2145, April 2002.

[68] X. Zhu and J. Kahn. Free-space optical communication through atmospheric turbulence channels. *IEEE Transactions on Communications*, August 2002.